A PHOTOELASTIC INVESTIGATION OF THERMAL STRESSES

LESTER H. BECK

A PHOTOELASTIC INVESTIGATION OF THERMAL STRESSES

*****

Lester H. Beck

A PHOTOELASTIC INVESTIGATION OF THERMAL STRESSES

by

Lester H. Beck II
Lieutenant Commander, United States Navy

Submitted in partial fulfillment of
the requirements for the degree of

MASTER OF SCIENCE
IN
MECHANICAL ENGINEERING

United States Naval Postgraduate School
Monterey, California

1958

A PHOTOELASTIC INVESTIGATION OF THERMAL STRESSES

by

Lester H. Beck

This work is accepted as fulfilling

the thesis requirements for the degree of

MASTER OF SCIENCE

IN

MECHANICAL ENGINEERING

from the

United States Naval Postgraduate School

ABSTRACT

This report describes a photoelastic technique for the evaluation of thermal stresses in models fabricated of Paraplex P-43. The optical and physical properties of this polyester resin were determined over the temperature range from room temperature to -40°F. Details of the techniques of casting and fabricating the models are given. Tuckerman optical strain gages were utilized in the determination of the modulus of elasticity and the thermal expansion coefficient.

Experimental investigations were conducted into the problems of an annulus contracting upon a steel plug, and the thermal stresses established by steady state heat transfer in a circular cylinder. The data obtained were correlated with theory utilizing the properties of the photoelastic material obtained in the calibration.

PREFACE

The work reported in this thesis was performed at the United States Naval Postgraduate School, Monterey, California, from January 1958 through May 1958.

The author wishes to express his appreciation to Professor Robert E. Newton for his guidance and assistance during all phases of the project, Mr. William C. Wixted of the Rohm and Haas Company who generously supplied the plastic materials used and provided much valuable technical assistance, and to his wife for her patience and her assistance with the photographic work.

SYMBOLS

Å	Wavelength-Angstrom Units (10^{-8}cm)
a	Inner radius of annulus or cylinder (in)
b	Outer radius of annulus or cylinder (in)
C	Material Fringe Constant (psi/fringe/in)
E	Modulus of Elasticity (psi)
f	Fringe order
K	Model Fringe Constant (psi/fringe)
P	Pressure (psi)
r	Radial coordinate (in)
t	Thickness of model (in)
α	Coefficient of Thermal Expansion (in/in-^{o}F)
Q	Photothermoelastic Figure of Merit (fringes/in-^{o}F)
$\frac{\Delta \ell}{\ell_o}$	Unit Elongation
ϵ	Strain
σ	Stress (psi)
ν	Poisson's Ratio

SUBSCRIPTS

Al	Aluminum
Cu	Copper
G	Gage
P	plastic
s	Steel
r	radial
t	tensile
$\ominus$	tangential
1	principal Directions
2	principal Directions

SUPERSCRIPT

'	Uncorrected Gage Reading

TABLE OF CONTENTS

LIST OF ILLUSTRATIONS

LIST OF TABLES

1. Introduction

The problem of thermal stresses in engineering structures has become one of increasing importance in recent years. Rockets, guided missiles, supersonic aircraft, and nuclear reactor heat exchangers are all instances where thermal stresses established by temperature gradients play an important part. Analytical solutions of the thermal stress problem, except for the simplest configurations, are likely to be quite involved and require some knowledge of the temperature distribution within the structure. Consequently, experimental verification of thermal stresses predicted by existing theory is of great value for the purposes of:

1. proving the applicability of the theory to the stated problem;
2. developing an experimental technique for those problems not easily solvable by theory.

Strain gage techniques, both electrical and optical, are complicated at the elevated temperatures generally associated with thermal stress determinations. The use of strain gages is limited to those locations on the surfaces of the body where it is possible to mount a gage.

Several attempts have been made to utilize the photoelastic technique in the analysis of thermal stresses. Rosenberg utilized the scattered light method and stress freezing technique to study a shrink fit model (1). The accuracy obtained was not as good as desired. Weibel (2,3) utilized Biot's dislocation method to construct a thermal stress analogy for a hollow circular cylinder and a square cylinder with a circular hole, under conditions of steady heat flow, which he analyzed photoelastically.

This method is, by its very nature, limited to certain applications and does not actually establish thermal stresses in the plastic model, but utilized the stresses introduced by the controlled displacement of two edges of an artifical slit in the model. These stresses are proportional to those which would occur in the original hollow cylinder.

It has long been known that the elastic behavior of plastic models varies as a function of temperature, the plastics being less brittle at higher temperatures. The material fringe constant (C) also varies as a function of temperature, increasing with an increase in temperature (4).

Gerard and Gilbert (5) utilized photoelastic techniques for the measurement of thermal stresses arising from transient temperature gradients, and from interference between mating elements of differing thermal expansion coefficients. Because of the creep characteristics of photoelastic materials at high temperatures, the temperature gradients were established by refrigeration. In order to evaluate the fringe patterns observed, and to correlate the experimental results with theory, the properties of the photoelastic material used were determined over a wide temperature range.

In determining the suitability of a plastic for use as a model in thermal stress determinations, Gerard and Gilbert defined a photothermoelastic figure of merit

$$Q_\alpha = \frac{\alpha E}{C}$$

where: -

α = thermal expansion coefficient of plastic, in/in$^{\circ}$F
E = modulus of elasticity of plastic, psi

The higher the value of Q_α, the more sensitive is the material

fringewise for a given thermal stress. On the basis of their initial tests they found that Paraplex P-43, a polyester resin manufactured by Rohm and Haas Company, had the highest figure of merit of the several materials tested. This material also has the advantage of being comparatively free of the time-edge effect and can be cemented to form complex structures. Subsequently additional materials have been tested which show promise as model materials for photo-thermoelastic stress determinations (6).

Utilizing P-43 as a model material Gerard and Gilbert (5) obtained good agreement with theory in solving the problems of a disc contracting upon an elastic inclusion and the transient thermal field produced by a sudden temperature differential applied to the upper edge of a long beam. More recently they investigated transient thermal stresses in I beams produced by a temperature differential suddenly applied at the top and bottom surfaces of the beam (7). Again, good agreement with the theory was obtained.

In evaluating a photoelastic technique for thermal stress analysis it is necessary to consider the application of the results obtained from the plastic models to the full scale structure. Because of the differences in thermal expansion coefficient and modulus of elasticity between the model and the prototype over differing temperature ranges, fairly elaborate thermal and geometrical scaling is necessary to apply model results to the prototype. The photoelastic method is valuable for quantitive evaluation of thermal stress theories and for providing a graphic, if not completely quantitative, solution to fairly involved problems under conditions of thermal and direct loading.

The purpose of this thesis is to verify the work of Gerard and Gilbert, giving detailed descriptions of the techniques involved in

the casting of Paraplex P-43, preparation of models, and the determination of the elastic and optical properties of the plastic. In order to assess the accuracy of the technique the problem of the disc contracting upon a steel plug in a uniform temperature field was solved experimentally and correlated with theory. In addition, an experimental investigation of the thermal stress problem of steady conduction through a circular cylinder was conducted and the results compared with theory.

2. Fabrication of Models.

A. Casting of Paraplex P-43.

Paraplex P-43 is a 70 percent solution of unsaturated polyesters in monomeric styrene. It is supplied by the Rohm and Haas Company in the form of a viscous liquid which may be cured to the solid state by the effect of catalysts and temperature. In Table 1 the physical properties of the uncured resin are given as supplied by Rohm and Haas (8).

Table 1

Properties of Paraplex P-43 Resin as Supplied

Monomer	Styrene
Polyester Concentration %	69-71
Viscosity	
Centipoises	2218-2765
Centistokes	1930-2410
Color-APHA	100 max
Specific Gravity (25°C.)	1.143-1.153
Refractive Index (N_D^{25})	1.5362
Acid Number (mg. KOH per gm.)	35 max
Flash Point	
(°C.)	54.4
(°F.)	130

The models used for determining the physical and optical properties of the material, as well as the model used in the shrinkage stress investigation, were machined from $\frac{1}{4}$ inch thick sheets of cured P-43.

The ¼ inch thick sheets were cast by pouring the catalyzed liquid monomer into a glass mold constructed of window glass with Plexiglass separators (9). This mold is shown assembled in Figure 1. The use of this glass mold produced sheets which required no further polishing. A detailed procedure, including recommended catalyst and accelerator concentrations, for casting Paraplex P-43 is given in Appendix II. The polymerization of P-43 is an exothermic reaction, and the internal heat developed must be dissipated rapidly in order to avoid cracking. For this reason, the amount of catalyst required will vary with the shape of the casting and with the mold material. This and other variables, such as amount of inhibiter in the resin, and air circulation in the curing oven, made the developing of a successful casting technique a long and arduous task.

The blanks, from which the circular cylinder model was machined, were cast utilizing the same general procedure outlined for the sheets. Because of the thickness of the piece (1½"), extreme care had to be taken to avoid cracking.

B. Machining the Models.

The models fabricated from the ¼ inch cast sheets (Figure 2) were roughout utilizing a jig saw. The tensile specimens were machined on a DuMore high speed grinder utilizing a ¼ inch diameter 48 tooth tungsten carbide cutter, operating at 22,000 RPM.

The cylindrical models were machined on a conventional metal lathe. The only model which required annealing after the machining operations was the 4" diameter by 1" thick cylinder. Details of the annealing and machining procedures are given in Part B of Appendix II.

Figure 1. Mold for Casting Plastic Sheets

Figure 2.
(left to right)
Template for Tension Model-Stepped Model for Fringe Constant-Annulus

C. Installation of Thermocouples.

In order to determine temperatures within the models it was necessary to cement thermocouples directly into the model. Copper-Constantan thermocouples of No. 30 wire (0.01") were used. Because of the low thermal conductivity of the model material, the smallest practicable size thermocouple wire was selected in order to minimize heat transfer through the wire itself.

The thermocouples were inserted in small holes drilled into the models and cemented in place using Paraplex P-43 as the cementing agent. The detailed procedures used for making the thermocouples and cementing them into the models are given in Part C of Appendix II.

3. Properties of Photoelastic Plastic.

To utilize Paraplex P-43 as a model material for investigating thermal stresses it is necessary to determine the modulus of elasticity, coefficient of thermal expansion and material fringe constant over the temperature ranges being investigated. The room temperature physical properties of cured Paraplex P-43, as given by the Rohm and Haas Company (8), are given in Table 2.

Table 2

Physical Properties of Cured Paraplex P-43 at 73.4°F

Ultimate strength (tension), psi.	9000
Elastic modulus (tension), psi.	5.9×10^5
Hardness-Rockwell M	110-120
Impact strength (Charpy unnotched), ft-lb per in	2.6
Polymerization shrinkage, % volume	7.0
Specific gravity	1.235
Thermal conductivity, Btu/ft^2-hr-°F/in	1.25
Specific heat, Btu/lb-°F	.32

A. Material Fringe Constant.

To provide the low temperatures required, a cold chamber was constructed of Styrofoam. The cold chamber is shown in position in the Chapman polariscope in Figure 3.

Styrofoam is an ideal material for equipment of this type. It is lightweight, waterproof, has excellent insulating properties, is machinable using woodworking tools, may be cemented with several common cements (10) and has sufficient structural stiffness not to require

Figure 3 Cold Chamber with Test Specimen in Position

additional reinforcement. The cold chamber was constructed of one inch thick Styrofoam with two inch thick pieces being utilized at the ends. The sections were assembled and glued with Weldwood glue, manufactured by the U.S. Plywood Corporation. The cold chamber was constructed with one face being removable to allow placement of the model and the refrigerant. The model is visible through a pair of double pane glass viewing windows. Each pane is 9" x 9" plate glass. Silica gel was used between each sheet to prevent fogging of the inner surfaces of the panes. The panes were cemented into the Styrofoam side panels with Elmer's Glue All Cement, manufactured by the Borden Company. The presence of four glass sheets, having a total thickness of one inch, in the optical path did not cause any disturbance in the optical path.

The refrigerating agent was dry ice pellets which were placed in a metal container in a separate section of the cold chamber. A small variable speed fan, powered by a 1/30 HB, 115V, 60 cycle capacitor motor, provided air circulation and uniform temperature distribution within the test section of the chamber. For the higher test temperatures, the heat absorption of the refrigerant was balanced by means of an electrical heating element mounted above the refrigerant container.

In all tests the temperature of the model was determined from thermocouples inserted in both ends of the specimen. The method of cementing the thermocouples is described in detail in Part C of Appendix II. A Rubicon potentiometer was used for measuring the thermocouple potentials. The ice junction was set in a glycerin-filled glass tube placed in a vacuum bottle filled with cracked ice. The ice junctions were dipped in General Electric Glyptal Enamel

(1201 red) to provide insulation and moisture-proofing.

Current to the electric heating element and the speed of the fan were controlled by two Superior Electric Company type 116 Powerstats, which could supply a voltage of from zero to 130.

The polariscope used in this investigation was a Chapman five inch research model polariscope manufactured by Chapman Laboratories. For observing the isochromatic fringe patterns a mercury vapor light source was used which, in combination with a green filter, provided a monochromatic light of 5461 Å. The polariscope is equipped with a three-inch field lens and has an 8" x 10" ground glass viewing screen and photographic plate holder. The loading frame supplied with this equipment is of the variable strain type. For this investigation, a dead weight loading frame was considered more suitable and was designed and built. The loading frame is shown in position in Figure 4 with a fringe constant test specimen in the cold chamber. The frame is designed for a maximum capacity of 1000 lbs. The fittings were designed to provide for the use of bending, as well as tensile test specimens, and to provide a range of lever ratios. The fulcrum of the lever arm is a steel pin fitted in a ball bearing which is, in turn, fitted into the lever arm.

In making the investigation of the material fringe constant (C), a stepped model, having three sections of separate cross sectional area (Figure 2), with imbedded thermocouples, was mounted on the loading frame inside the cold chamber. (Figure 3). The lever arm was adjusted for a 3:1 ratio. Silica gel was placed in the bottom of the chamber to reduce moisture condensation. The refrigerant container was filled with dry ice, and the front side of the cold chamber fastened into place. The electric fan was then started to

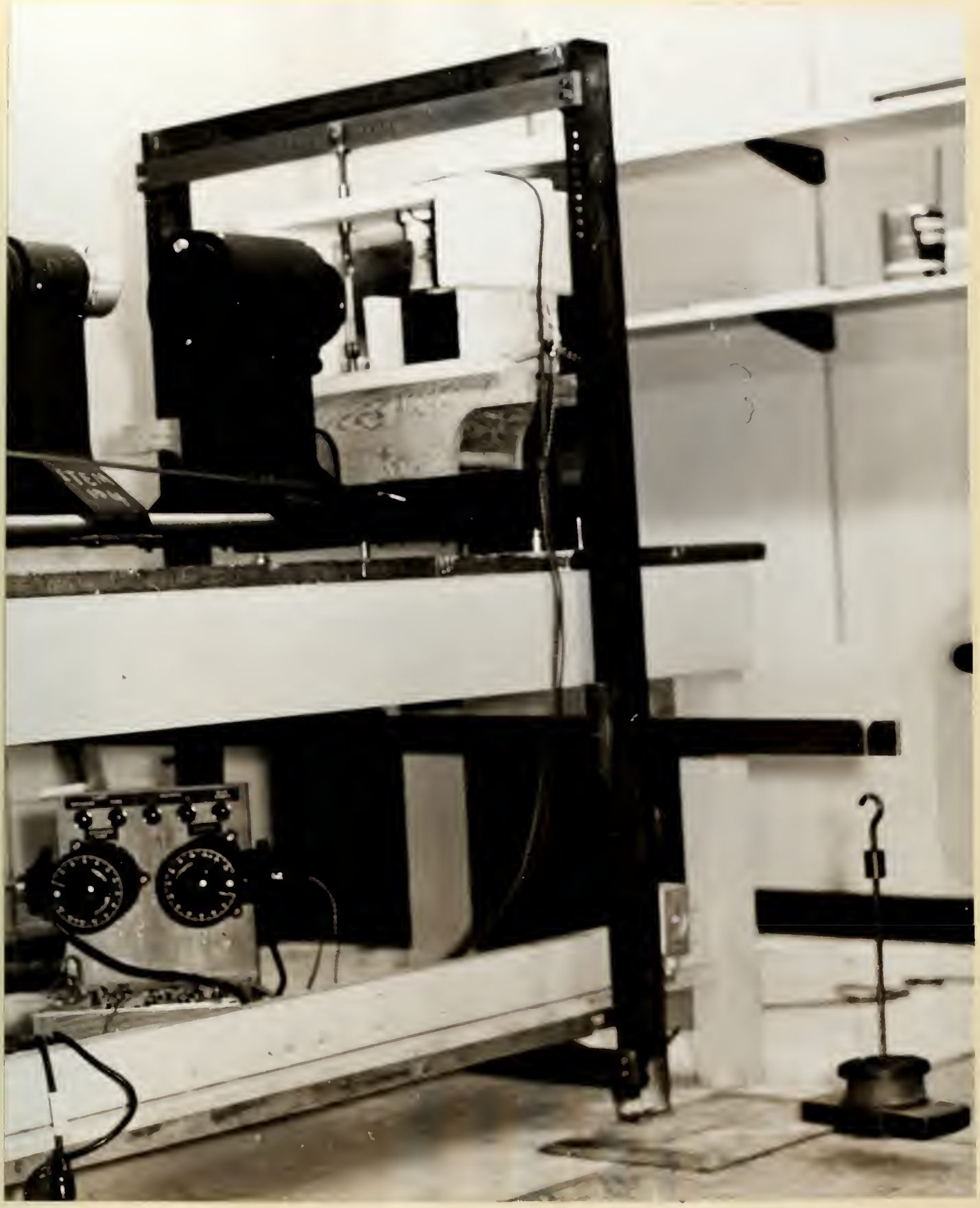

Figure 4 Loading Frame and Polariscope

provide air circulation and the heater adjusted to provide stabilization at the temperature desired. When temperature equilibrium was obtained, as evidenced by uniform temperatures throughout the model and the air adjacent to the model, the specimen was brought to a uniform darkness. The load was recorded and loading continued, recording the loads required to produce successive fringes in the three sections of the specimen. After sufficient data were obtained, the temperature in the cold chamber was changed and the procedure repeated for other temperatures.

For each temperature, fringe order (f) was plotted against tensile stress (σ_t) and the slope obtained. For pure tension the difference in principal stresses ($\sigma_1 - \sigma_2$) is equal to σ_x since σ_2 is equal to zero. The difference in principal stresses ($\sigma_1 - \sigma_2$) corresponding to each isochromatic fringe order is given by $(\sigma_1 - \sigma_2) = \sigma_t = \frac{fC}{t}$ (11) for a model of thickness (t). The slope of the fringe order versus tensile stress plot is $\frac{\sigma_t}{f} = \frac{C}{t} = K$

where K is the model fringe constant. The values of the material fringe constant (C) obtained at various temperatures are plotted in figure 5.

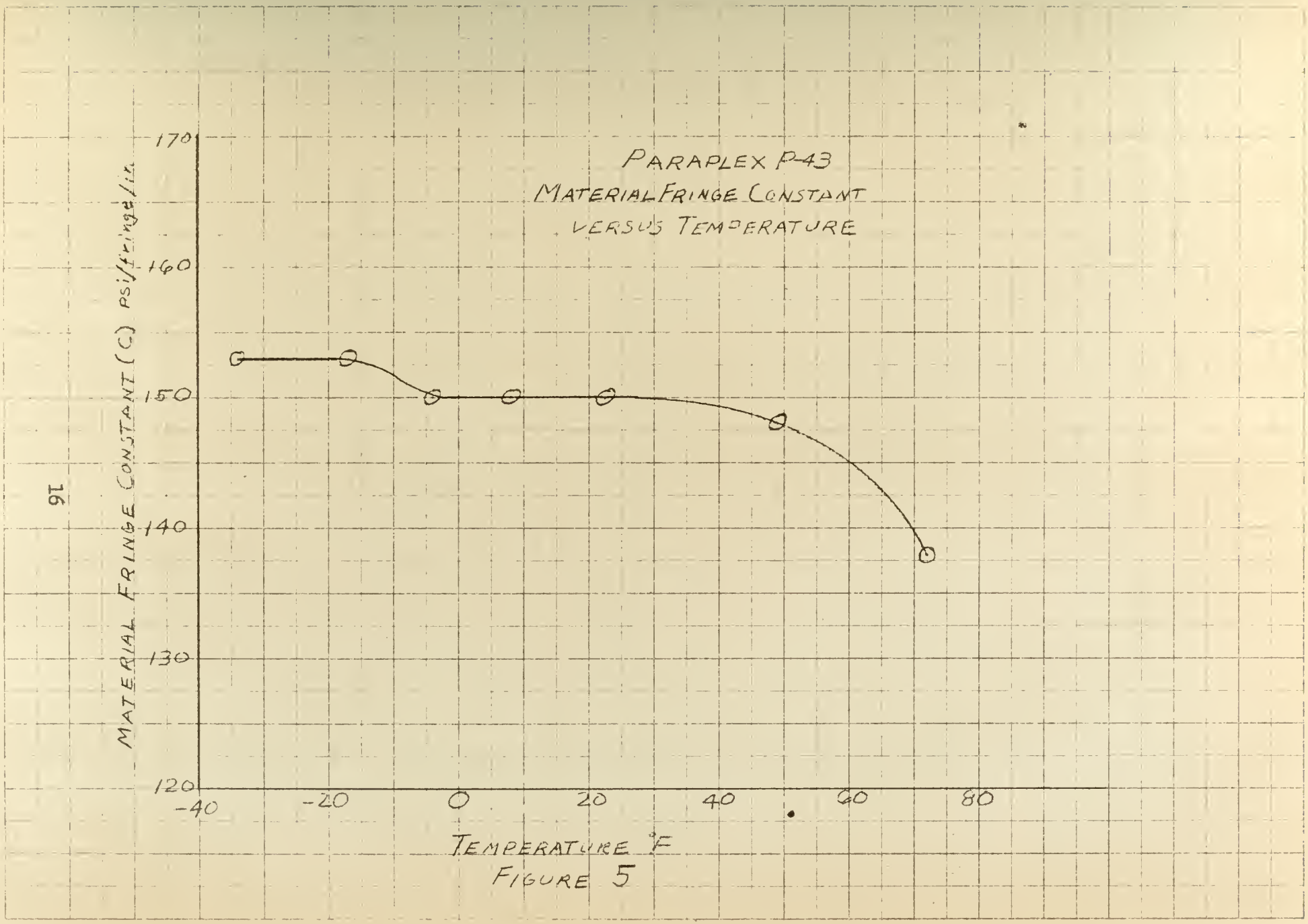
PARAPLEX P-43
MATERIAL FRINGE CONSTANT
VERSUS TEMPERATURE
MATERIAL FRINGE CONSTANT (C) PSI/FRINGE/IN.
170
160
150
140
130
120
-40
-20
0
20
40
60
80
TEMPERATURE °F

FIGURE 5

B. Modulus of Elasticity.

The modulus of elasticity (E) was determined from stress-strain data obtained from tensile tests conducted over the same temperature range (-40°F to 72°F) as that employed in obtaining the material fringe constant. The template used in machining the tensile test model is shown in Figure 2. The loading machine and cold chamber were used as described in the previous section. To provide accurate strain data, Tuckerman optical strain gages were used.

The Tuckerman optical strain gage, manufactured by the American Instrument Company, is of the triple reflection mechanical-optical type, and consists of two basic parts: the auto-collimator and the extensometer or gage. These two components are shown in Figure 6. The gage is capable of measuring strains of 2×10^{-6} in/in with a one inch gage length. The theory and a detailed description of the equipment is given by Tuckerman in his report describing the original instruments (12), and in the manufacturer's instruction books (13). The gage was fastened to the tensile specimen with two Neg'ator constant force springs. The clamping force applied was approximately one pound; which is that recommended by Wilson for optimum results (14).

Two thermocouples were cemented into the tensile test specimen, one at each end. In addition, a thermocouple was installed so that the junction indicated the surface temperature of the gage. Thermal equilibrium was considered established only when both thermocouples mounted in the specimen, and the thermocouple indicating the gage temperature gave potential readings which differed by less than an amount corresponding to 1°F. Because of the low thermal conductivity of P-43, considerable time was required to reach equilibrium. In order to avoid errors arising from differential expansion between the gage

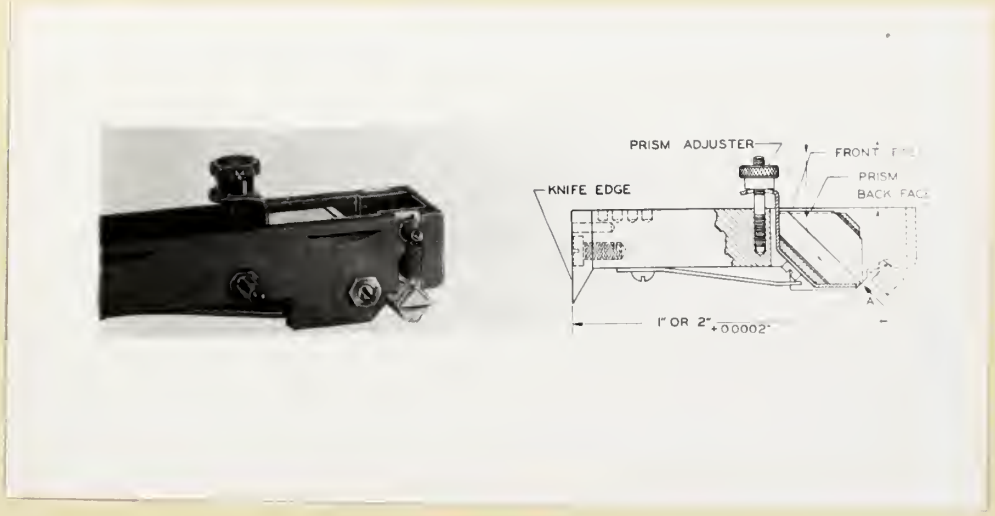

Gage or Extensometer

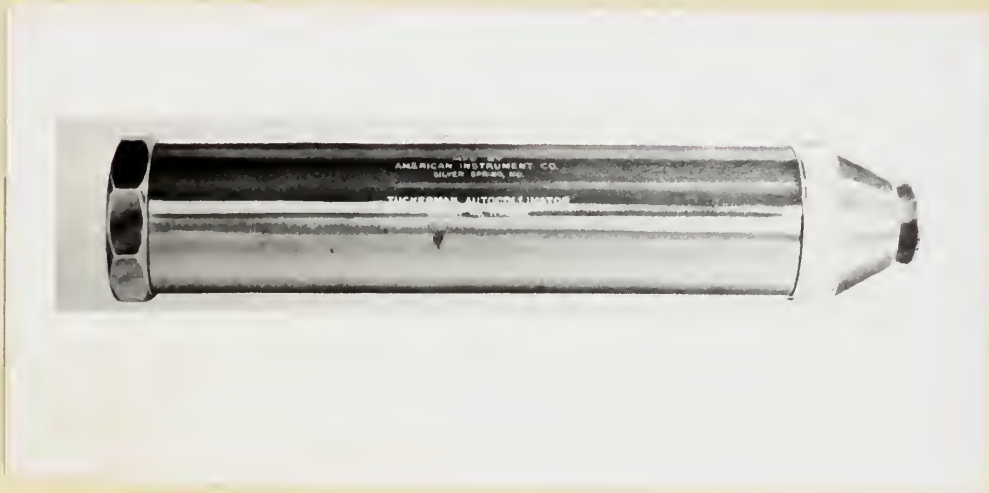

Auto-collimator

Figure 6 Tuckerman Optical Strain Gage

and model, it was essential that the gage and specimen be at the same temperature.

The gage was read through the window of the cold chamber, utilizing the auto-collimator. The double windows of the cold chamber presented no difficulties in reading the gage except for the presence of additional flash images. Difficulty was experienced, at temperatures in the vicinity of $32^{\circ}F$, with moisture condensation on the gage optics. Condensation was avoided by the use of liberal quantities of activated Silica-Gel on the floor of the cold chamber and by keeping entirely above or below the condensation temperature, when making a series of runs, until after the desired data had been obtained.

The modulus of elasticity (E) was obtained from conventional stress-strain plots for each temperature. The values obtained for modulus of elasticity versus temperature are plotted in Figure 7.

The time under applied load was kept to a minimum (approximately one minute at each stress level) to reduce any possible creep effects. The tensile testing of plastic materials is complicated by the variation of the elastic properties with degree of polymerization, time rate of loading and total elongation (15). Because of this, it is important that the calibration procedure be followed each time a model is made from a new sheet of resin, and that a standardized procedure be adopted for performing the calibration.

C. Thermal Expansion Coefficient.

The procedure and apparatus used in the determination of the thermal expansion coefficient (α_p) for the model material was the same as that outlined for determining the modulus of elasticity except that no load was applied to the specimen, and a correction factor was applied to account for differential expansion between

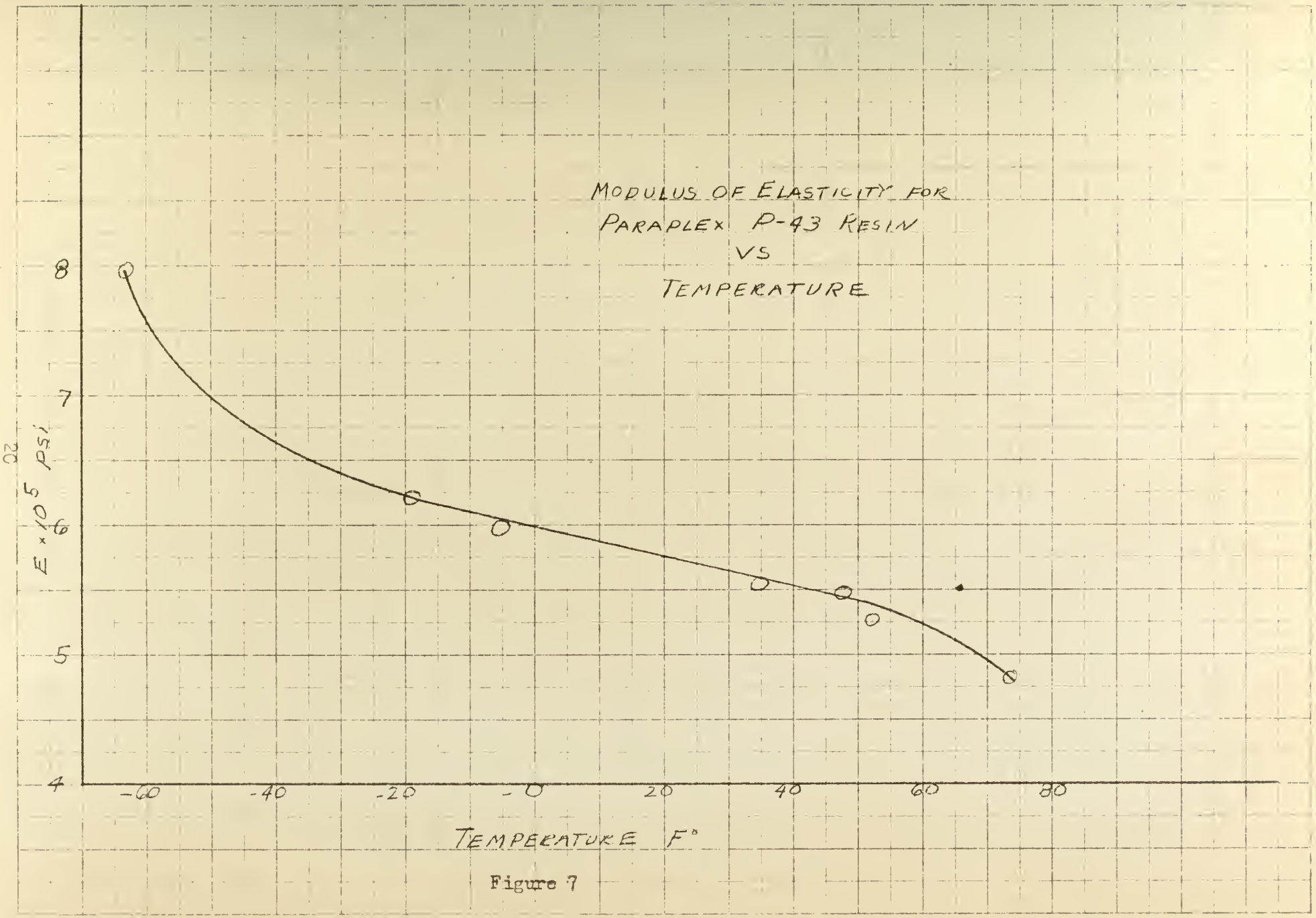
MODULUS OF ELASTICITY FOR
PARAPLEX P-43 RESIN
VS
TEMPERATURE
E × 10^5 psi
8
7
6
5
4
-60
-40
-20
-0
20
40
60
80
TEMPERATURE F°

Figure 7

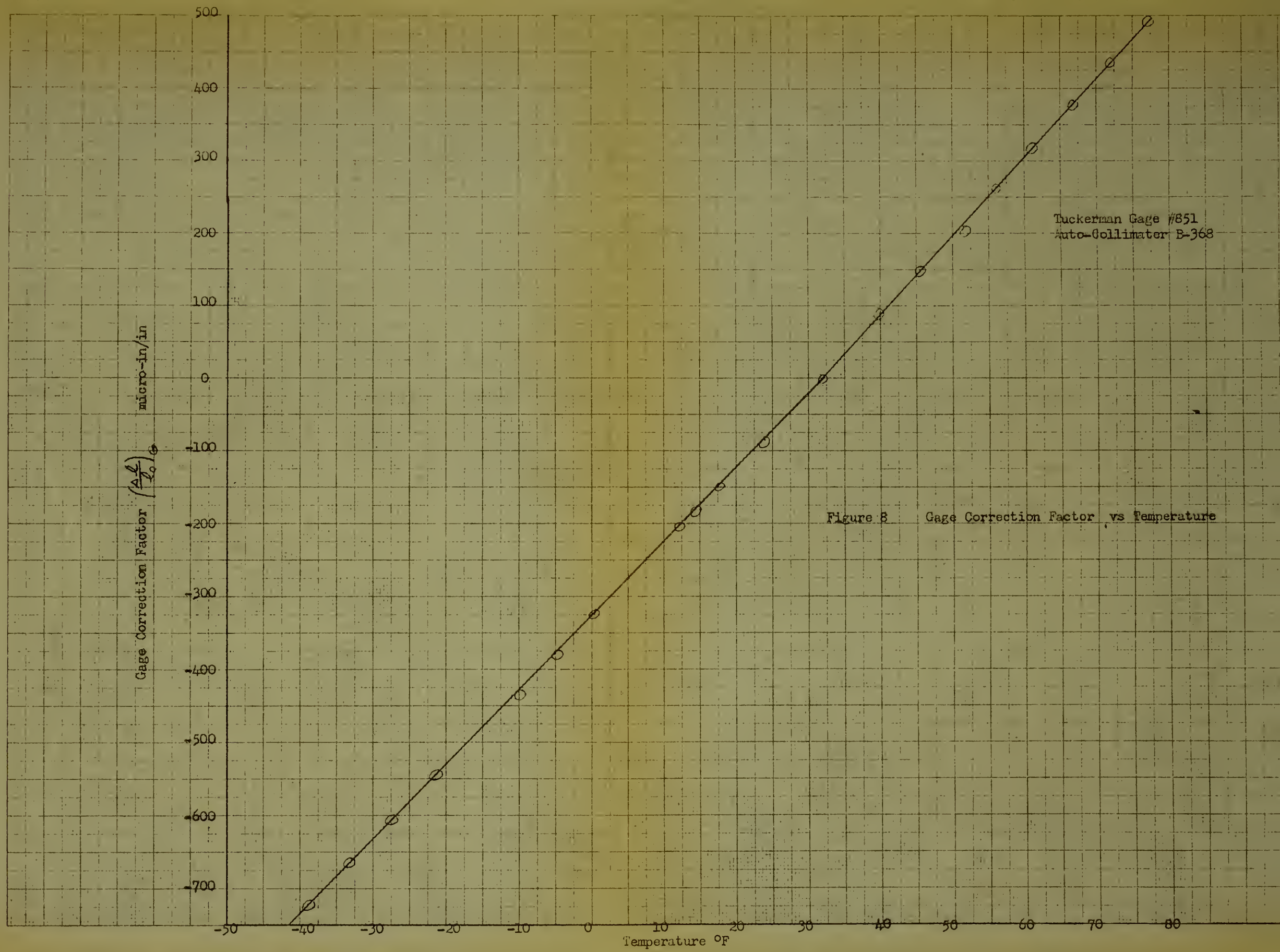

Figure 8 Gage Correction Factor vs Temperature

the gage and the model as temperature was varied.

In order to determine the correction factor to be applied, the gage was calibrated over the desired temperature range by obtaining a plot of unit elongation $\left(\frac{\Delta l}{l_o}\right)_{Cu}$ versus temperature (T) for copper. Copper was selected for the calibration specimen because: its $\left[\left(\frac{\Delta l}{l_o}\right)_{Cu}\right]$ has been accurately measured over the entire temperature range being considered; its expansion properties are least affected by small amounts of impurities; and it is more readily obtained in a relatively pure state than the other common metals. The gage correction factor $\left[\left(\frac{\Delta l}{l_o}\right)_G\right]$ was obtained by adding the value of the unit elongation $\left[\left(\frac{\Delta l}{l_o}\right)'_{Cu}\right]$ as obtained directly from the gage readings, to the standard values for copper $\left(\frac{\Delta l}{l_o}\right)_{Cu}$ obtained by Nix and MacNair (16).

$$\left(\frac{\Delta l}{l_o}\right)_G = \left(\frac{\Delta l}{l_o}\right)_{Cu} + \left(\frac{\Delta l}{l_o}\right)'_{Cu}$$

The gage correction factor is shown plotted as a function of temperature in Figure 8.

The unit elongation $\left[\left(\frac{\Delta l}{l_o}\right)_P\right]$ was then obtained for Paraplex P-43 over the same temperature range and corrected by the addition of the gage correction factor.

$$\left(\frac{\Delta l}{l_o}\right)_P = \left(\frac{\Delta l}{l_o}\right)'_P + \left(\frac{\Delta l}{l_o}\right)_G$$

The corrected values of $\left[\left(\frac{\Delta l}{l_o}\right)_P\right]$ were plotted as a function of temperature and are shown in Figure 9. The thermal expansion coefficient (α_p), which is the slope of the $\left(\frac{\Delta l}{l_o}\right)_P$ versus temperature curve, was found to have a constant value of 28.2×10^{-6} in/in-^oF in the temperature range from -40^oF to 32^oF and a value of 36.5×10^{-6} in/in-^oF in the range from 32^oF to room temperature.

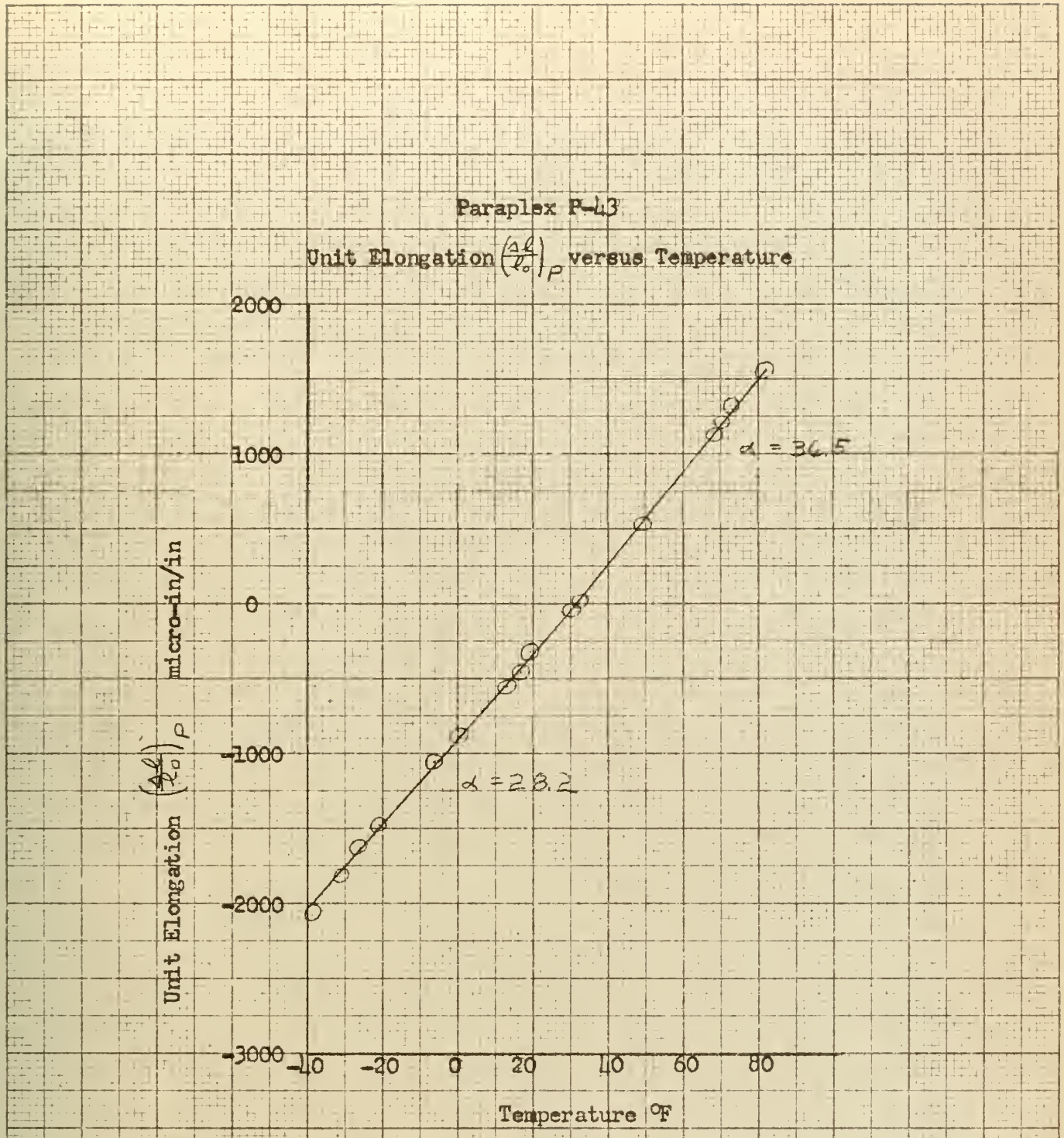

Figure 9 Unit Elongation versus Temperature

A check run was made utilizing a 61ST-T6 aluminum alloy sample to obtain values of $(\frac{\Delta l}{l_o})'_{Al}$ at various temperatures and applying the gage correction factor to get corrected values of the unit elongation. The thermal expansion coefficient obtained from the $(\frac{\Delta l}{l_c})_{Al}$ versus temperature plot agreed very closely with the published values (17) for the temperature range investigated.

4. Analysis of Thermal Stresses in an Annulus due to Interference.

The first quantitative check of the photoelastic technique for thermal stress determination was for the problem of a plastic annulus contracting upon a steel plug inserted into the central hole with a nug fit. Upon lowering the temperature 100°F, the greater thermal expansion coefficient (α_p) of the plastic, as compared with that of the steel, caused the plastic annulus to contract upon the steel plug, establishing a pressure (p) between the outside of the plug and the inside of the annulus. The stress field arising from this internal pressure was investigated by photoelasticity, and the results correlated with theory.

A. Theory.

The interface pressure (p) between a circular annulus of inner radius (a) and outer radius (b) fitted with a central steel plug is a function of the temperature change (ΔT) and is expressed as: (18)

$$P = \frac{(\alpha_p - \alpha_s)\Delta T E_p E_s (b^2 - a^2)}{(1-\nu_s)E_p(b^2-a^2) + E_s[(1-\nu_p)b^2 + (1+\nu_p)a^2]}$$

where E_p = Modulus of elasticity of P-43, psi
E_s = Modulus of elasticity of steel, psi
α_p = Thermal expansion coefficient for P-43, in/in-°F
α_s = Thermal expansion coefficient for steel, in/in-°F
ν_p = Poisson's ratio for P-43
ν_s = Poisson's ratio for steel

The principal stresses at any radial location (r) due to this pressure are: (19)

σ_r = radial-stress = $\frac{a^2 p}{b^2-a^2}\left[1 - \frac{b^2}{r^2}\right]$
σ_θ = tangenial-stress = $\frac{a^2 p}{b^2-a^2}\left[1 + \frac{b^2}{r^2}\right]$

The difference in principal stresses is given by:

$$\sigma_\theta - \sigma_r = \frac{2p}{\left[1-\left(\frac{a}{b}\right)^2\right]\left(\frac{r}{a}\right)^2}$$

The fringe order (f) is;

$$f = (\sigma_\theta - \sigma_r)\frac{t}{C}$$

where t = Thickness of model, in
C = Material fringe constant, psi/fringe/in

Combining the two previous equations, we obtain:

$$f = \frac{2pt}{\frac{r^2}{a^2} C\left[1-\left(\frac{a}{b}\right)^2\right]}$$

Solving for r we obtain the theoretical radius at which the fringe of order f will appear.

$$r = \left[\frac{2pta^2}{fC\left[1-\left(\frac{a}{b}\right)^2\right]}\right]^{\frac{1}{2}}$$

B. Experimental Procedure.

A plastic annulus was machined, as described in Part B of Appendix II, from the same sheet of Paraplex that was used to obtain the optical and physical properties given in the previous section. The annulus is shown in Figure 2. A steel plug was inserted into the central hole of the annulus with a snug fit (zero clearance) and the unit was placed in the cold chamber and polariscope as shown in Figure 10. Thermocouples were cemented in both the plastic and the plug. The temperature of the assembly was lowered 100°F and the fringe photograph shown in Figure 11 obtained.

C. Results and Comparison.

The following values, obtained from the calibration data, were used in the equations given in Part A of this section;

$\alpha_p = 28.2 \times 10^{-6}$ in/in-°F
$\alpha_s = 7.0 \times 10^{-6}$ in/in-°F
$E_p = 6.25 \times 10^5$ psi
$E_s = 30 \times 10^6$ psi

Figure 10 Annulus Fitted With Steel Plug

Figure 11 Fringe Photograph, Annulus Contracting Upon a Steel Plug

$C = 153$ psi/fringe/in
$\nu_p = .36$
$\nu_s = .29$

The model dimensions were:

$a = .375$ in
$b = 1.25$ in
$t = .250$ in

The initial temperature (T_1) and final temperature (T_2) determined experimentally were:

$T_1 = 75^{\circ}F$
$T_2 = -25^{\circ}F$
$\Delta T^2 = 100^{\circ}F$

The above values were substituted into the applicable equations in Part A of this section and gave a value of p of 1560 psi. Theoretical curves were obtained for fringe order (f) versus radius and for principal stress difference ($\sigma_\theta - \sigma_r$) as a function of the radius. These curves are given in Figures 12 and 13 together with the experimental points obtained from the fringe photograph. It can be observed that good agreement was obtained.

The waviness of the isochromatic fringes in the photograph is believed to be largely due to frictional effects at the contacting surfaces. These effects are most evident in the fringes nearest the central hole of the annulus. An additional factor, that may cause fringe pattern distortion, is slight variations of the optical properties of the plastic within the model.

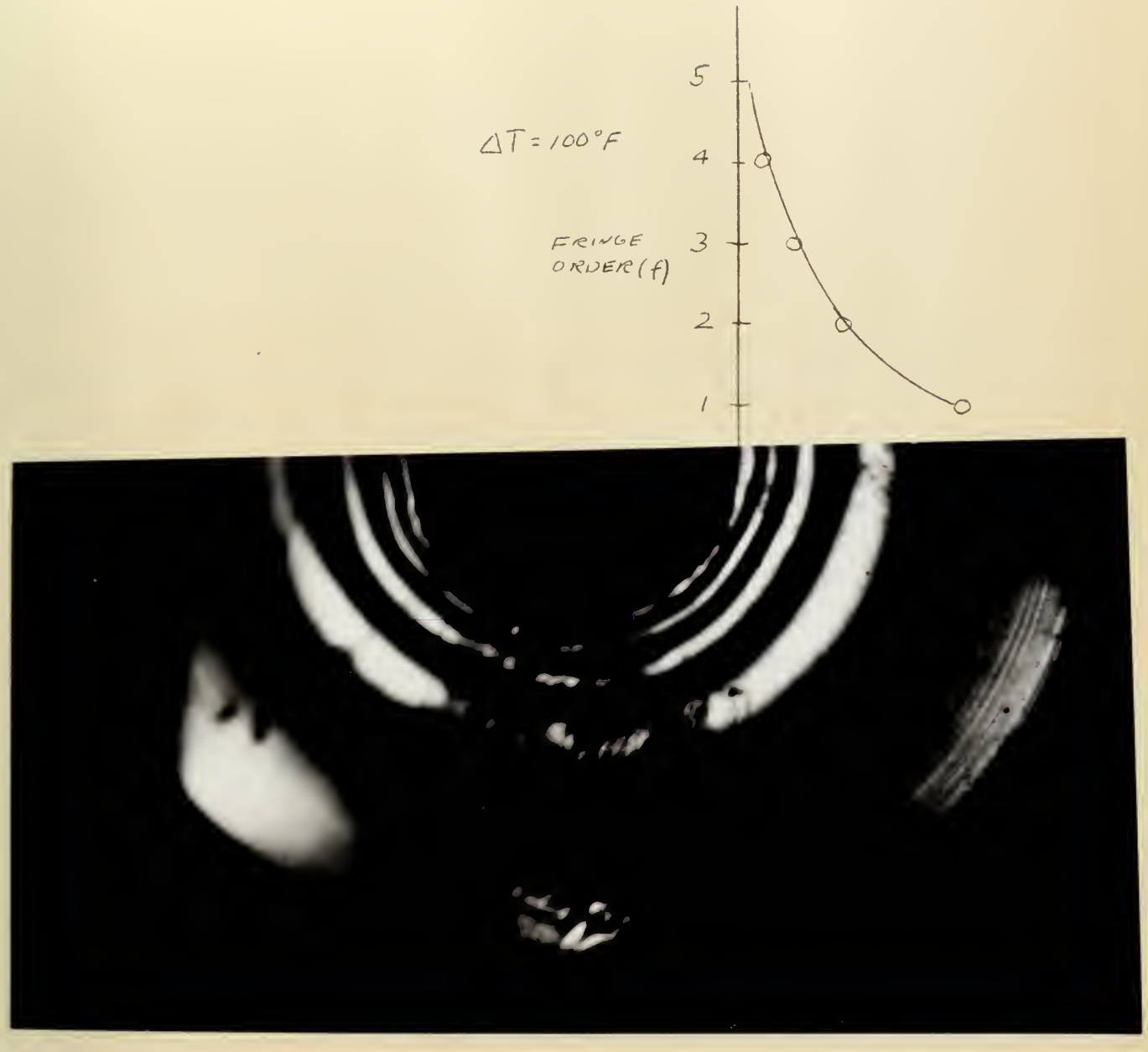

Figure 12 Fringe Photograph of an Annulus Contracting Upon a Steel Plug. Test points are observed fringe orders. The solid line represents computed values of fringe order versus radius. Dark field. Magnification: 2.66

Annulus Contracting Upon a Steel Plug

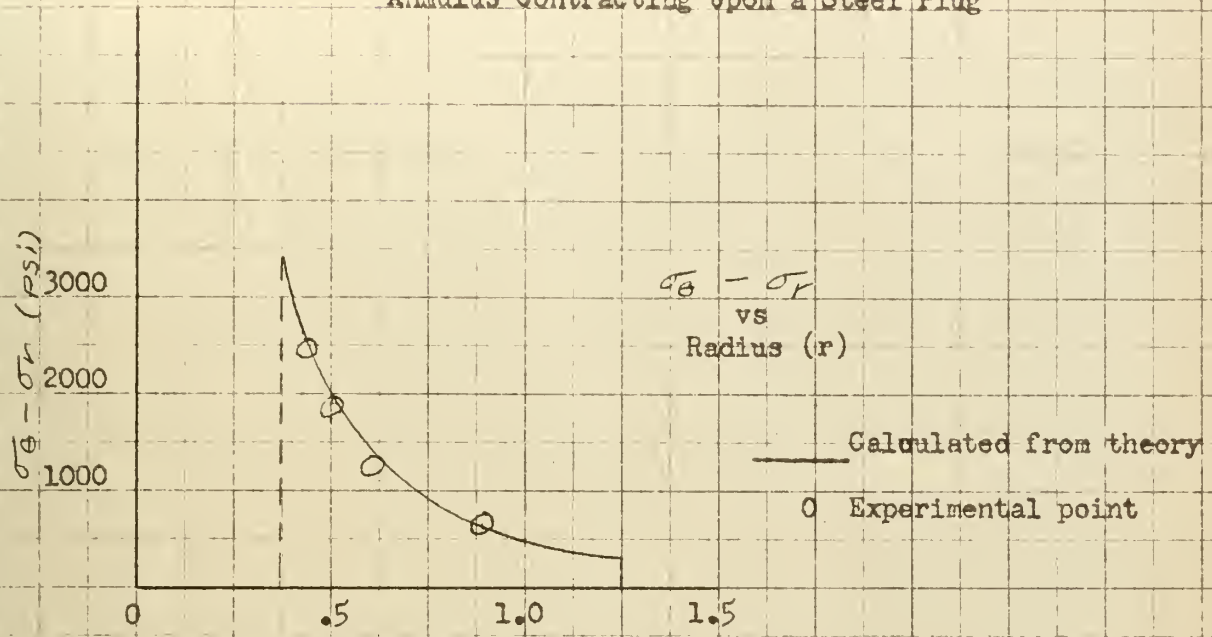

Figure 13a

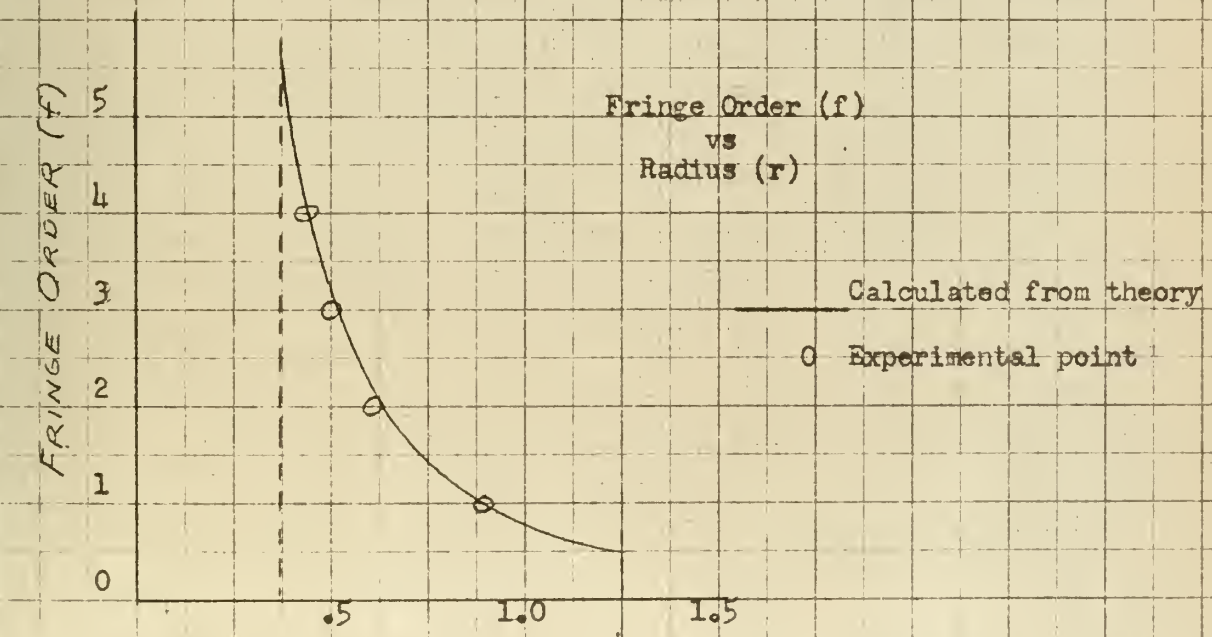

Figure 13b

5. Analysis of Steady State Thermal Stresses in a Circular Cylinder.

The second application of the photoelastic technique for thermal stress determination was to the problem of steady state radial conduction through a hollow circular cylinder. A low temperature was maintained on the outer surface of the cylinder by means of powdered dry ice. The inner surface was maintained at an approximately constant temperature by means of cold water flowing through the central hole. When steady state conditions were established, the isochromatic fringe pattern caused by the thermal stresses within the cylinder was photographed. The absolute value of the difference in principal stresses ($|\sigma_\theta - \sigma_r|$) was obtained from the fringe photograph and compared with a theoretical solution based upon the measured radial temperature distribution within the model.

A. Theory.

Convective heat transfer from the air to the faces of the cylinder causes a temperature gradient to be established across the thickness of the model. This temperature gradient will introduce a difference in stress across the thickness and the polariscope actually is sensitive to an average value of stress through the thickness. An analytical solution for the stress distribution in this case is difficult to attain. Therefore, for purposes of comparison with the experimental results, the model was considered to be in a state of plane stress. In deriving the expressions for the stresses it was assumed that; (20) the cylinder was in a state of plane stress with radial symmetry; and that, temperature is a function of radius alone.

For the plane stress case the thermal stresses are given by (20)

$$\sigma_r = \frac{-\alpha E}{r^2}\int_a^r Tr\,dr + \frac{E}{1-\nu^2}\left[C_1(1+\nu) - C_2(1-\nu)\frac{1}{r^2}\right]$$

$$\sigma_\theta = \frac{\alpha E}{r^2}\int_a^r Tr\,dr - E\alpha T + \frac{E}{1-\nu^2}\left[C_1(1+\nu) + C_2(1-\nu)\frac{1}{r^2}\right]$$

Applying the boundary conditions that the radial stress (σ_r) be equal to zero on the inner and outer surfaces of the cylinder, (when r = a and r = b) we obtain:

$$\sigma_r = -\frac{\alpha E}{r^2}\int_a^r Tr\,dr + \frac{E\alpha}{b^2-a^2}\int_a^b Tr\,dr\left[1 - \frac{a^2}{r^2}\right]$$

$$\sigma_\theta = \frac{\alpha E}{r^2}\int_a^r Tr\,dr - E\alpha T + \frac{E\alpha}{b^2-a^2}\int_a^b Tr\,dr\left[1 + \frac{a^2}{r^2}\right]$$

Solutions for the principal stresses as a function of radius were obtained utilizing graphical integration of a Tr versus r curve which was obtained from the temperature distribution obtained experimentally.

B. Experimental Procedure.

A 4 inch OD by 1 inch thick circular cylinder with a 1 inch diameter central hole was cast and machined as described in Appendix II. Three thermocouples were cemented into the model at a depth of .8" at locations indicated in Figure 14. It was assumed that the temperature distribution through the thickness of the model was symmetrical with respect to the axis through the center of the thickness. Assuming a parabolic distribution, a point .3 in. from the center line approximates the location of the average temperature through the thickness.

The model was mounted in a Plexiglass box, supported by flexible Mylar film to avoid placing any restraints on the outside of the cylinder. The cylinder mounted in the Plexiglass

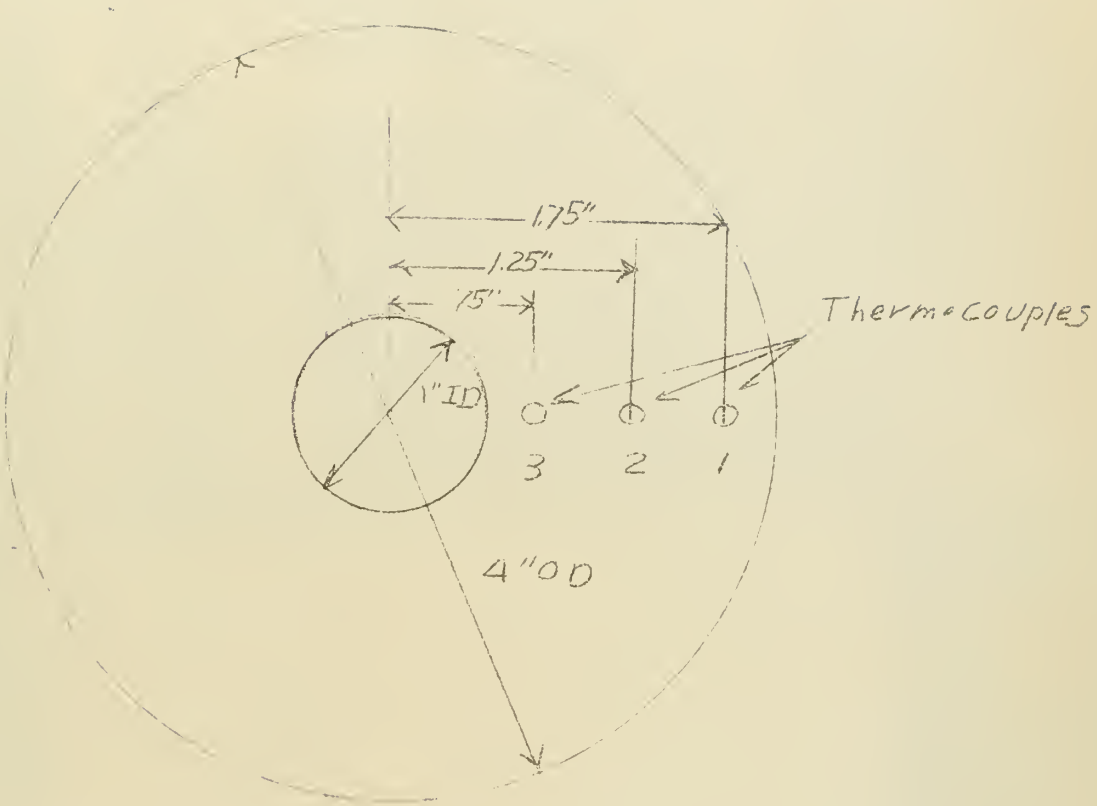

Figure 14 Circular Cylinder Model Showing Location of Thermocouples

Figure 15 Cylinder Mounted in Plexiglass Box

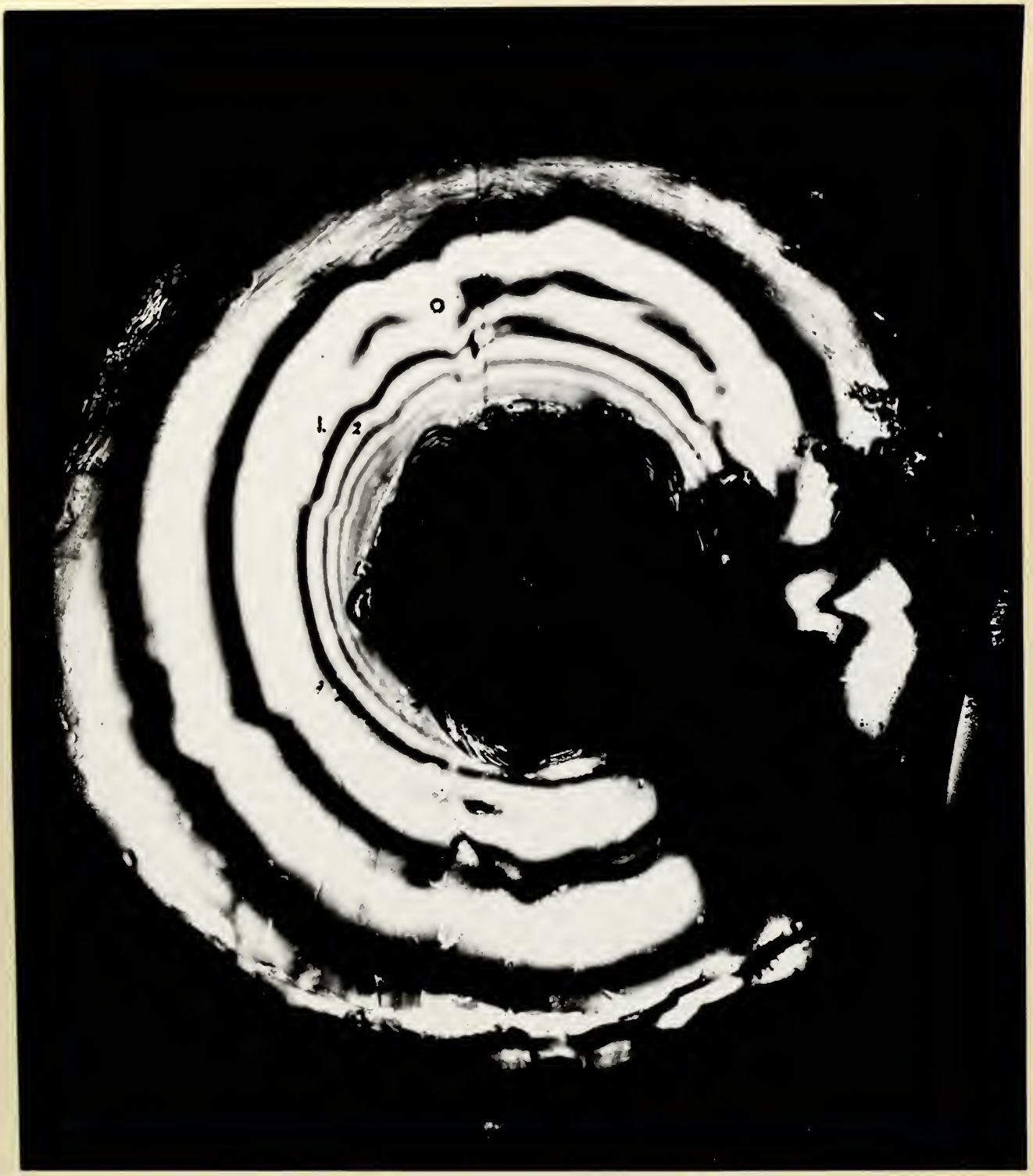

Figure 16 Isochromatic Fringe Pattern-Circular Cylinder With Steady State Conduction. Dark Field.

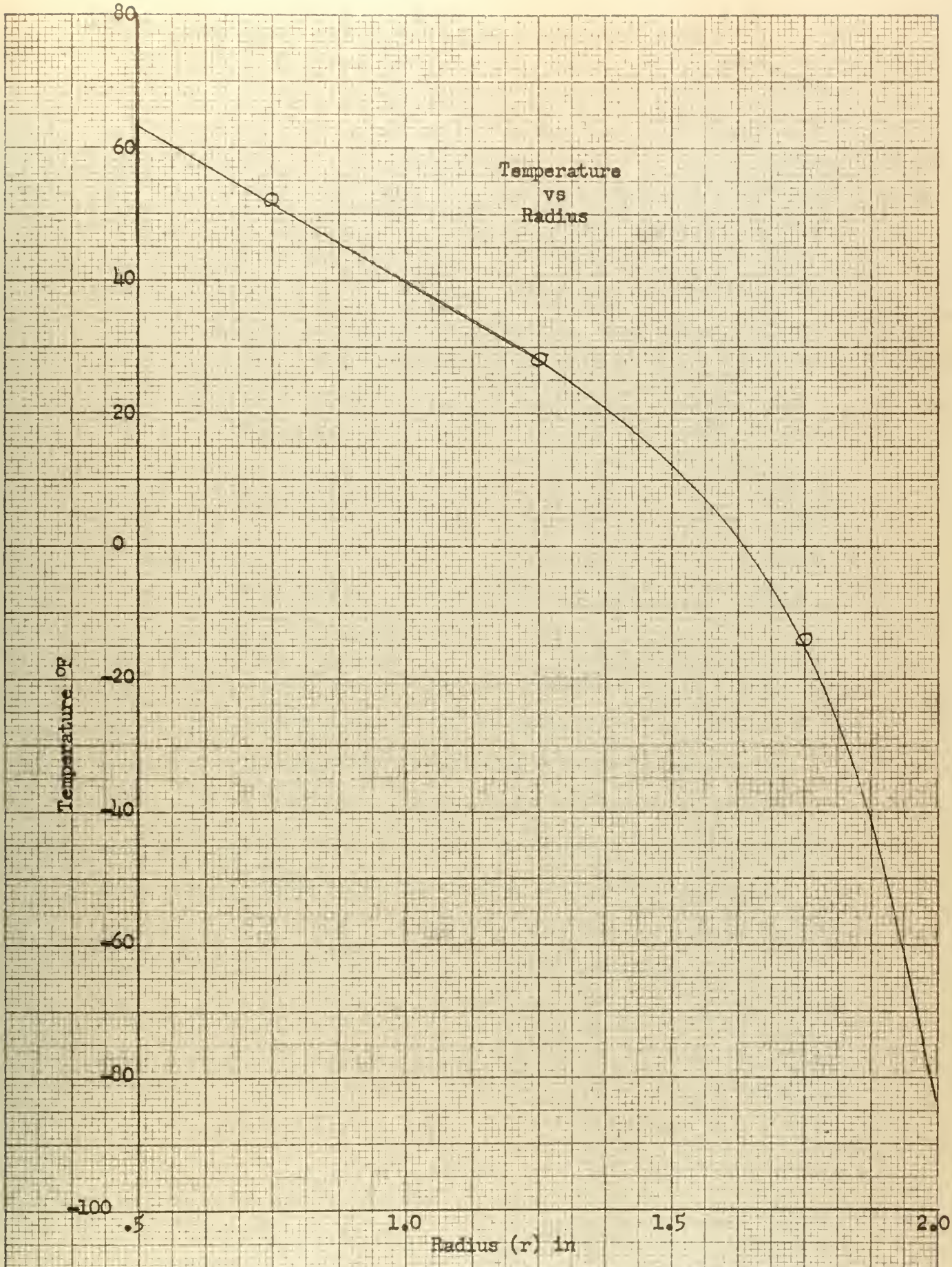

Figure 17 Temperature Distribution in Circular Cylinder Steady State Conduction

box is shown in Figure 15. Mylar film remains flexible at dry ice temperatures and was easily cemented to both the P-43 model and the Plexiglass box. Dupont #4684 cement was used, along with the (P-43-P-13) cement described in Part D of Appendix II.

The temperature distribution was established by filling the Plexiglass box with finely powdered dry ice and by circulating tap water through the central hole of the cylinder. When steady state conditions were reached, the isochromatic fringe pattern was photographed (Figure 16) and the temperatures recorded. The zero order fringe was located by viewing the model with circularly polarized white light.

C. Results.

A curve of temperature versus radius was obtained from the observed steady state temperature distribution (Figure 17). A curve of Tr versus r was obtained and integrated, using Simpson's method, to obtain a curve of $\int_a^r Tr\,dr$ versus r. Using this and values of E and α for P-43 from the calibration curves, a plot of the absolute value of principal stress difference ($|\sigma_\theta - \sigma_r|$) versus radius was obtained for the plane stress case. The absolute value of $|\sigma_\theta - \sigma_r|$ was computed inasmuch as observed fringe orders are inherently positive and from observation of fringe pattern alone the sign of $\sigma_\theta - \sigma_r$ can not be determined. The theoretical plot of $|\sigma_\theta - \sigma_r|$ versus r, along with the experimental points obtained from the fringe photograph, are given in Figure 18. The following is a sample calculation of the principal stresses for r = .75 in.

From Calibration Curves	From Model
α_{AV} = 33 x 10^{-6} in/in-^oF	a = .5"
E_{AV} = .6 x 10^6 psi	b = 2"

From observed temperature distribution assuming outer edge at 0^o T = 135 $\int_a^b Tr\,dr = 169$ $\int_a^r Tr\,dr = 21.5$

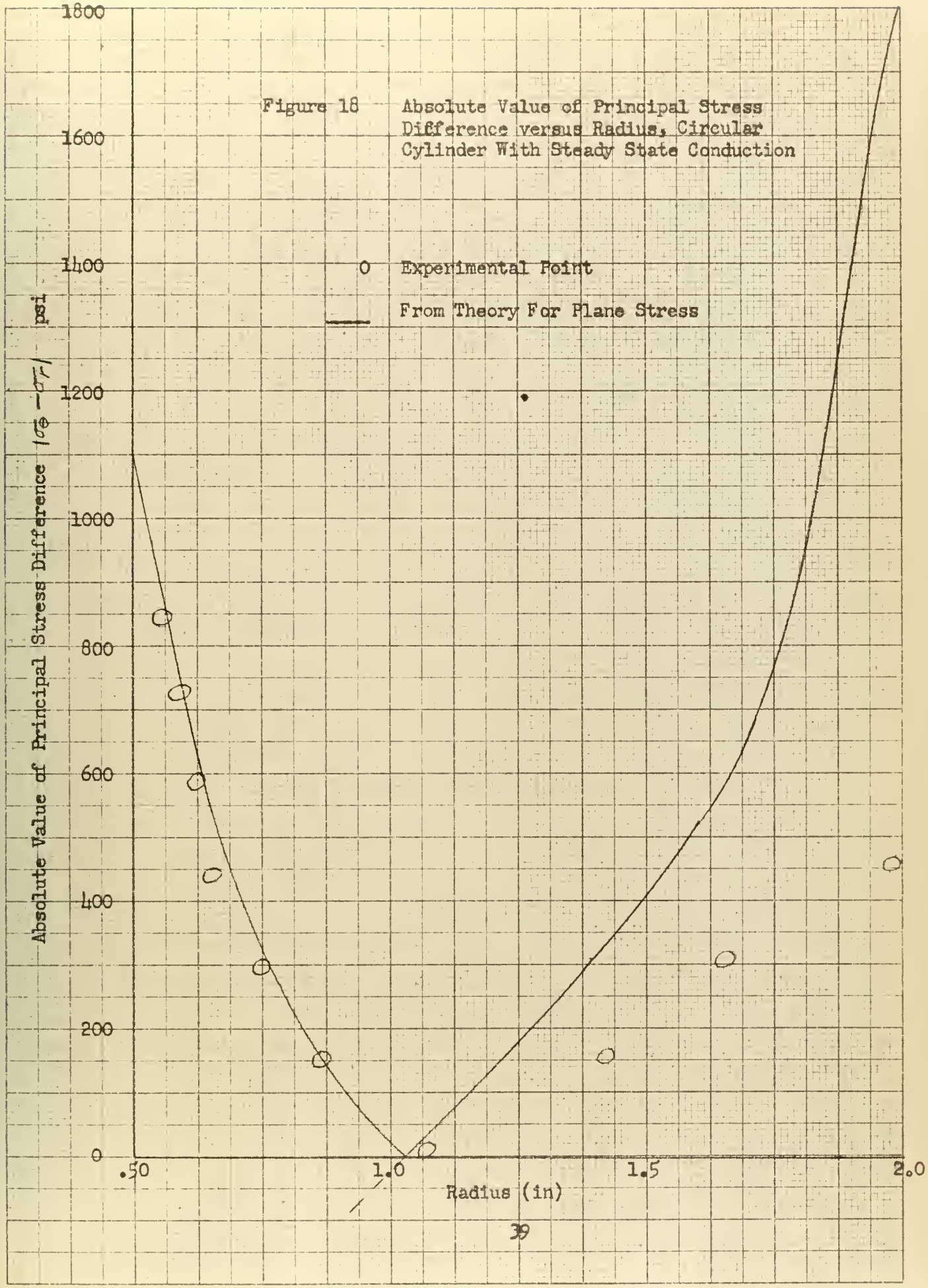

Figure 18 Absolute Value of Principal Stress Difference versus Radius, Circular Cylinder With Steady State Conduction

$$\sigma_r = \frac{-\alpha E}{r^2}\int_a^r T r\,dr + \frac{E\alpha}{b^2-a^2}\int_a^b T r\,dr\left[1-\frac{a^2}{r^2}\right]$$

$$\sigma_r = \frac{-33\times 6}{.75^2}\times 21.5 + \frac{33\times 6}{3.75}\times 169\left[1-\frac{.25}{.75^2}\right] = -289\ psi$$

$$\sigma_\theta = \frac{\alpha E}{r^2}\int_a^r T r\,dr - \alpha E T + \frac{E\alpha}{b^2-a^2}\int_a^b T r\,dr\left[1+\frac{a^2}{r^2}\right]$$

$$\sigma_\theta = \frac{33\times 6}{.75^2}\times 21.5 - 33\times 6\times 135 + \frac{33\times 6}{3.75}\times 169\left[1+\frac{.25}{.75^2}\right] = -620\ psi$$

$$\sigma_\theta - \sigma_r = -331\ psi \qquad |\sigma_\theta - \sigma_r| = 331\ psi$$

Fairly good agreement with the theoretical solution for the plane stress case was obtained near the inner surface of the cylinder. Toward the outer surface the experimental results differ considerably from theory. This divergence from theory is believed to be due to the increasing temperature gradient across the thickness of the cylinder as the outer edge is approached. This temperature gradient introduces a difference in stresses across the thickness of the model. It was assumed in deriving the expressions for the principal stresses that:

1. the temperature does not vary over the thickness of the model;

2. the stress does not vary over the thickness of the cylinder.

Both these assumptions are violated in the model; however, the temperature gradient across the model near the inner surface was considered comparatively small and good agreement was obtained with the experimental results.

A theoretical solution, based on the observed temperature distribution, was also obtained assuming the model to be in a state of plane strain. This solution differed considerably from that obtained experimentally.

6. Conclusions.

The photoelastic technique for evaluating thermal stresses appears to have excellent possibilities as a quantitative means for verifying theoretical solutions of thermal stress problems.

The principal limitations of the method appear to be the extensive calibration procedure required for the model material and the difficulties associated with the casting of models from the liquid resin.

More specific conclusions are:

1. The work of Gerard and Gilbert in calibrating the Paraplex P-43 models was verified. It appears that the modulus of elasticity and the thermal expansion coefficient will vary with curing procedures, necessitating the calibration of the material for each individual application.

2. Good agreement with theory was obtained for the case of a plastic annulus contracting upon a steel plug when subjected to a temperature change. This correlation validated the calibration technique.

3. Results obtained from the experimental evaluation of steady state thermal stresses in a circular cylinder indicate the applicability of the photoelastic technique to problems where an analytical solution may not readily be obtainable.

BIBLIOGRAPHY

1. P. R. Rosenberg, Study of a Shrink Fit Model by the Scattered Light Method. Proc. 13th Semiannual Eastern Photoelasticity Conf, MIT, June 1941, pp. 99-103.

2. E. E. Weibel, Thermal Stresses in Cylinders by the Photoelastic Method, Proc. 5th. Int. Cong. App. Mech., Cambridge, 1938.

3. S. Timoshenko and J. N. Goodier, Theory of Elasticity, McGraw-Hill, 1951, pp. 428-433.

4. G. H. Lee and C. W. Armstrong, Effect of Temperature on Physical and Optical Properties of Photoelastic Materials, Jour. App. Mech., Vol. 5 No. 1, pp. A11-12, March 1938.

5. G. Gerard and A. C. Gilbert, Photo-Thermoelasticity: An Exploratory Study, NYU Coll. of Eng. Research Report SM56-11, May 1956.

6. H. Tramposch and G. Gerard, The Physical Properties of Several Materials for Use in Photo-Thermoelastic Investigations, NYU Coll. of Eng. Research Report SM57-5, May 1957.

7. H. Tramposch and G. Gerard, Photo-Thermoelastic Investigation of I Beams, NYU Coll. of Eng. Research Report SM58-1, Jan. 1958.

8. Rohm and Haas Company, Paraplex P-Series Resins, 94 pp., 1956.

9. J. O. Beattie, Casting Plastic Sheets, Modern Plastics, pp. 109-117, July 1956.

10. Dow Chemical Company, Styrofoam-Fabrication, Adhesives and Coatings, Dow Bulletin 171-42E, 5th Edition, December 1956.

11. G. H. Lee, An Introduction to Experimental Stress Analysis, Wiley, 1950.

12. L. B. Tuckerman, Optical Strain Gages and Extensometers, Proc. ASTM, Vol. 23, Part II, p. 602, 1923.

13. American Instrument Company, Instructions for Tuckerman Optical Strain Gages.

14. B. L. Wilson, Characteristics of the Tuckerman Strain Gage, Proc. ASTM, Vol. 44, pp. 1017-1026, 1944.

15. F. W. Reinhart, Tension Testing of Plastics, Symposium on Tension Testing of Non-Metallic Materials, ASTM Special Tech. Pub. 194, pp. 3-18, 1957.

16. F. C. Nix and D. MacNair, the Thermal Expansion of Pure Metals, Physical Review, Vol. 60, pp. 597-605, Oct. 15 1941

17. American Society for Metals, Metals Handbook, 1948, p. 822.

18. R. V. Southwell, An Introduction to the Theory of Elasticity, Second Edition, Oxford, pp. 406-407, 1941.

19. Timoshenko and Goodier, op. cit., p. 60.

20. ibid., pp. 406-408.

21. M. M. Frocht, Photoelasticity, Wiley, pp. 342-345, 1941.

22. H. Baker, E. Ryder, and N. Baker, Temperature Measurement in Engineering, Vol. 1, Wiley, pp. 48-49, 1953.

23. W. C. Wixted, Private Communication, December 1958.

24. Rohm and Haas Company, Technical Bulletin No. 337, Sept. 1957.

GENERAL REFERENCES

1. E. Coker and L. Filon, A Treatise on Photoelasticity, Cambridge, 1931

2. M. Hetenyi, Handbook of Experimental Stress Analysis, Wiley, 1950.

3. R. Heywood, Designing by Photoelasticity, Chapman & Hall, 1952.

4. J. Jaeger, On Thermal Stresses in Circular Cylinders, Philosophical Magazine, Vol. 36, No. 257, pp. 418-428, June 1945.

5. W. McAdams, Heat Transmission, Third Edition, McGraw-Hill, 1954.

6. H. Walton, Plastics for the Home Craftsman, McGraw-Hill, 1951.

APPENDIX I

SUMMARY OF EXPERIMENTAL DATA

A. Material Fringe Constant

$T = -34^{\circ}F$

Load P (lb)	Fringe Order f	Area in^2	Stress σ_t (psi)
25	1	.0414	604
50.5	2	.0414	1218
35.1	1	.0567	617
69.0	2	.0567	1215

From plot C = 153 psi/f/in

$T = -16^{\circ}F$

Load P (lb)	Fringe Order f	Area in^2	Stress σ_t (psi)
24	1	.0414	580
36.7	1	.0567	620
49.5	2	.0414	1195
68.0	2	.0567	1200
74.5	3	.0414	1807

C = 153 psi/f/in

$T = -3.8^{\circ}F$

Load P (lb)	Fringe Order f	Area in^2	Stress σ_t (psi)
19.5	1	.0425	458
29.1	1	.0586	496
45.0	2	.0425	1058
45.0	1	.0908	496
66.0	2	.0586	1125
68.1	3	.0425	1600

C = 150 psi/f/in

T = 8°F

Load P (lb)	Fringe Order f	Area in^2	Stress σ_x (psi)
19.5	1	.0425	459
29.1	1	.0586	496
44.4	2	.0425	1042
51.0	1	.0908	561
66	2	.0586	1126
67.5	3	.0425	1588

C = 150 psi/f/in

T = 22.5°F

Load P (lb)	Fringe Order f	Area in^2	Stress σ_x (psi)
18.3	1	.0425	430
29.7	1	.0586	506
44.7	2	.0425	1051
47.1	1	.0908	518
64.5	2	.0586	1100
67.5	3	.0425	1588

C = 150 psi/f/in

T = 49°F

Load P (lb)	Fringe Order f	Area in^2	Stress σ_x (psi)
24.3	1	.0414	587
36.0	1	.0567	634
48.0	2	.0414	1160
70.2	2	.0567	1238
72.0	3	.0414	1740

Load P (lb)	Fringe Order f	Area in^2	Stress σ_x (psi)
4.8	1	.0414	116
11	1	.577	192.5
30	2	.0414	725
30	1	.091	330
43.5	2	.0577	754
52.5	3	.0414	1268
75.0	3	.0577	1300
75.0	4	.0414	1810
82.5	2	.091	907

C = 138 psi/f/in

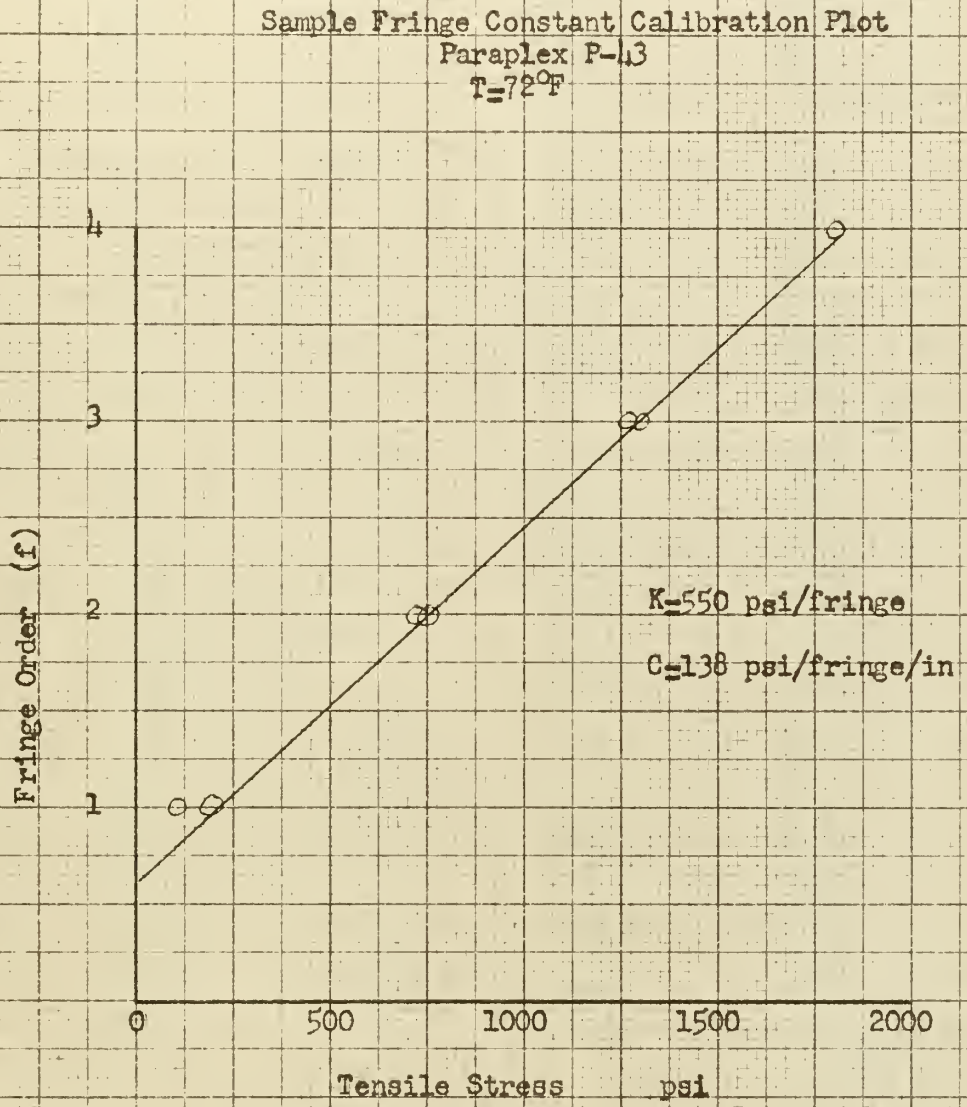

Figure 19 Sample Fringe Constant Calibration Plot

B. Modulus of Elasticity.

Temp. F^{o}	Load P (lb)	Area in^2	Stress σ_ε (psi)	Strain ε in/in x 10^6	
-63	30	.234	128	88	
"	60	"	256	200	
"	90	"	384	308	
"	120	"	512	436	
"	150	"	640	588	$E=7.9 \times 10^5$psi
-19	30	.234	128	300	
"	60	"	256	572	
"	90	"	384	768	
"	120	"	512	968	
"	150	"	640	1182	
"	166.5	"	711	1288	
"	183	"	782	1408	
"	199.5	"	854	1530	
"	216	"	923	1638	
					$E=6.21 \times 10^5$psi
-5	30	.234	128	306	
"	60	"	256	564	
"	90	"	384	754	
"	120	"	512	960	
"	150	"	640	1178	
"	166.5	"	711	1304	
"	183	"	782	1424	
"	199.5	"	854	1540	
"	216	"	923	1664	
					$E=5.97 \times 10^5$psi
34.5	30	.234	128	336	
"	60	"	256	588	
"	90	"	384	790	
"	120	"	512	1034	
"	150	"	640	1272	
"	166.5	"	712	1398	
"	183	"	782	1528	
"	199.5	"	854	1658	
"	216	"	923	1782	
"	232.5	"	995	1904	
					$E=5.54 \times 10^5$psi

Temp. F^{o}	Load P (lb)	Area in^2	Stress σ_x (psi)	Strain ϵ in/in x 10^6
47.5	30	.234	128	316
"	60	"	256	596
"	90	"	384	856
"	120	"	512	1050
"	150	"	640	1280
"	166.5	"	712	1434
"	183	"	782	1570
"	199.5	"	854	1708
"	216	"	923	1856
"	232.5	"	995	1978
				$E=5.14 \times 10^5$psi
52.0	30	.234	128	346
"	60	"	256	652
"	90	"	384	882
"	120	"	512	1118
"	150	"	640	1352
"	166.5	"	712	1492
"	183	"	782	1644
"	199.5	"	854	1770
"	216	"	923	1890
				$E=5.26 \times 10^5$psi
75.0	30	.234	128	178
"	60	"	256	450
"	90	"	384	710
"	120	"	512	968
"	150	"	640	1246
				$E=4.82 \times 10^5$psi

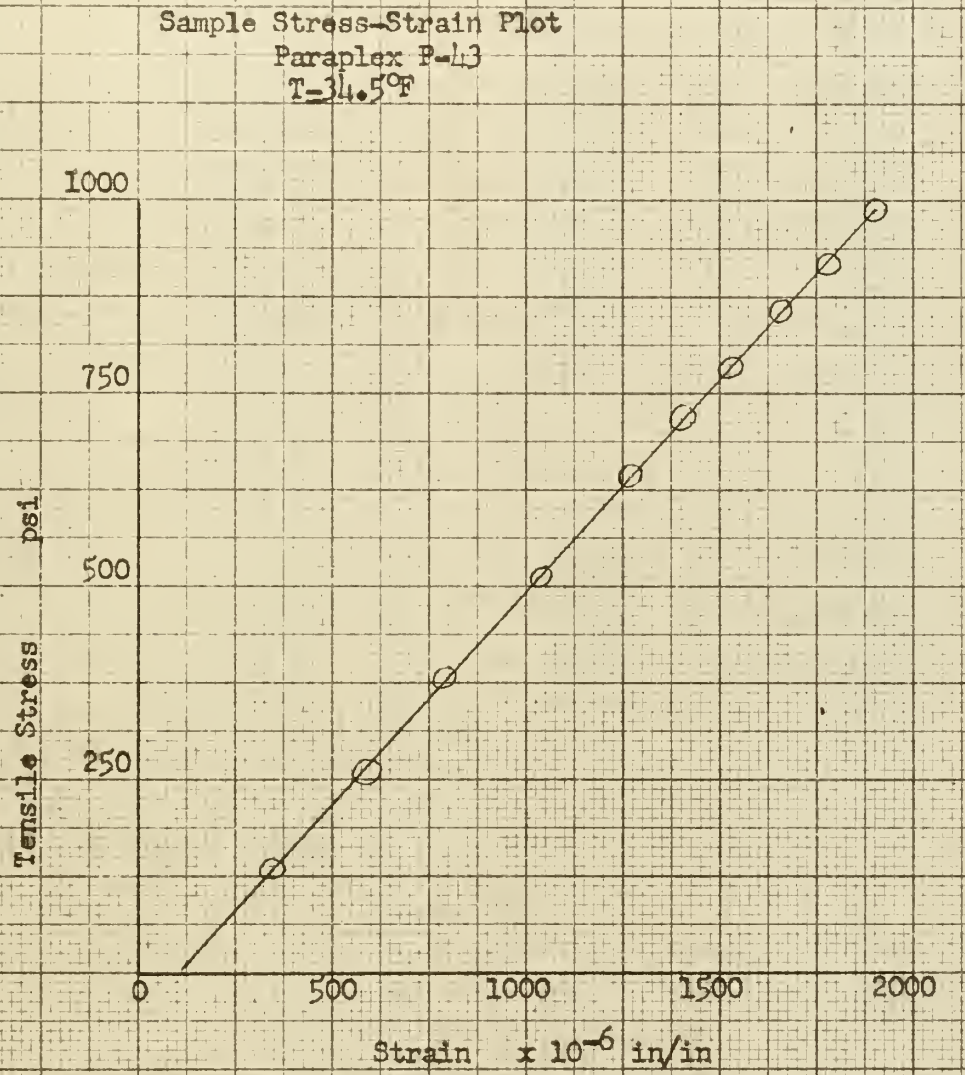

Figure 20 Sample Plot, Stress vs Strain

C. Determination of Gage Correction Factor for Tuckerman Gage #851

Temp. °F	$\left(\frac{\Delta l}{l_o}\right)'_{Cu}$	$\left(\frac{\Delta l}{l_o}\right)_{Cu}$	$\left(\frac{\Delta l}{l_o}\right)_{G}$
	x 10^6	x10^6	x 10^6
-47.2	-87.2	-696.5	-783.7
-39.0	-79.3	-642.5	-721.8
-33.0	-72.9	-591.1	-664.0
-27.6	-67.0	-539.7	-606.7
-21.4	-61.1	-488.3	-549.4
-16.6	-56.6	-436.9	-493.5
-9.8	-49.3	-385.5	-434.8
-4.6	-44.0	-334.1	-378.1
.2	-39.0	-282.7	-321.7
5.9	-31.7	-231.3	-263.0
12.2	-24.0	-179.9	-203.9
17.6	-17.3	-128.5	-145.8
23.9	-10.0	- 77.1	- 87.1
29.3	- 3.0	- 25.7	- 28.7
32.0	0	0	0
34.7	3.0	25.7	28.7
39.6	11.1	77.1	88.2
45.5	16.2	128.5	144.7
51.8	24.0	179.9	203.9
56.2	29.5	231.3	260.8
60.8	36.1	282.5	318.6
66.6	43.7	334.1	377.8
71.8	51.2	385.5	436.7
77.0	58.4	432.6	491.0

D. Determination of $\left(\frac{\Delta l}{l_o}\right)_P$ for Paraplex P-43.

Temp °F	$\left(\frac{\Delta l}{l_o}\right)'_P$ x 10^6	$\left(\frac{\Delta l}{l_o}\right)_G$ x 10^6	$\left(\frac{\Delta l}{l_o}\right)_P$ x 10^6
-39.0	-1290	-722	-2012
-31.6	-1164	-647	-1811
-25.5	-1024	-585	-1609
-21.0	- 946	-540	-1486
- 6.0	- 678	-387	-1065
- .8	- 566	-318	- 884
13.3	- 366	-192	- 558
16.3	- 292	-160	- 452
19.1	- 184	-132	- 316
30.6	- 32	- 12	- 44
49.3	350	188	538
65.2	676	363	1039
68.4	736	395	1131
70.4	780	417	1197
74.5	968	462	1430
82.0	1006	545	1551

E. Plastic Annulus Contracting Upon a Steel Plug.
Data Obtained from Fringe Photograph

f	r (in.)	$\sigma_\theta - \sigma_r$ (psi)	$\sigma_\theta - \sigma_r$ (calc) psi
1	.884	612	617
2	.605	1224	1320
3	.500	1835	1930
4	.430	2445	2620

Model Dimensions; C = 153 psi/f/in

a = .375"
b = 1.25"
t = .25"

F. Steady State Thermal Stresses in a Circular Cylinder

a. Temperature Distribution

Thermocouple	r (in.)	Temp. °F.
1.	1.75	-14.5
2.	1.25	24.0
3.	.75	52.2

b. Data Obtained from Fringe Photograph

f	r (in)	C(psi/f/in)	$\lvert\sigma_\theta - \sigma_r\rvert$ psi
6	.554	144	864
5	.594	144	720
4	.602	145	580
3	.647	146	437
2	.750	147	294
1	.863	148.5	148.5
0	1.07		0
1	1.43	150	150
2	1.66	150	300
3	1.98	153	459

c. Calculation of $\sigma_\theta - \sigma_r$ from Observed Temperature Distribution.

r(in)	T	$\int_a^r Tr\,dr$	σ_θ (psi)	σ_r (psi	$\lvert\sigma_\theta - \sigma_r\rvert$ (psi)
.5	146	0	-1100	0	1100
.625	140.5	10	-809	-184	625
.75	135	21.5	-620	-289	331
1.0	124	50	-350	-319	31
1.125	118	66	-235	-312	77
1.25	111.5	84	-102	-316	214
1.50	95	119	160	-250	410
1.75	68	149.5	585	-145	730
2.0	0	169	1792	0	1792

APPENDIX II

Detailed Procedures for Fabrication of Models

A. Casting of Paraplex P-43

The models used for determining the physical and optical properties of the plastic material, as well as the model used in the shrinkage stress investigation, were machined from $\frac{1}{4}$ inch thick sheets of P-43. Several considerations enter into the design of a suitable mold for casting the plastic in sheet form. During the polymerization phase of its cure the resin gives off a considerable amount of heat. Unless this heat is dissipated rapidly, cracking of the resin will result. In order to minimize this effect the first mold constructed was of aluminum. It was found that the cured plastic was difficult to separate from the mold and that a good surface finish was not obtained. A glass mold was then designed and constructed of two pieces of 9" x 11" double strength window glass with strips of $\frac{1}{4}$ inch Plexiglass as a separator (9). The mold, consisting of the two pieces of glass separated by the Plexiglass separator or gasket, was then clamped together by spring-type stationary clamps as shown in Figure 1. The use of this glass mold produced sheets which required no further polishing.

Polymerization of P-43 may be initiated by several combinations of accelerators and catalysts and at both room and elevated temperatures. In general, these combinations may be classified as room temperature catalysts and elevated temperature catalysts.

room temperature catalysts investigated included methyl ethyl katone peroxide accelerated with Accelerator "B", and with 6 percent cobalt naphthenate solution. Benzoyl peroxide was used where heat could be applied early in the cure cycle. The concentrations of catalyst and accelerator required proved quite difficult to determine. Since the resin cures in bulk, the exothermic heat of polymerization must be dissipated rapidly in order to avoid cracking. For this reason, the amount of catalyst required will vary with the shape of the casting and with the mold material. The highest concentrations of catalyst are used in applications where the resin will be used in the form of a thin film as a cement, and the lowest where a fairly large disc or block is being cast. Table 3 gives combinations of catalysts and curing cycles which gave the best results for the applications outlined.

Table 3

Recommended Catalyst and Cure Combinations

Paraplex P-43

Catalyst	Accelerator	Cure	Applications
benzoyl perox. .5% (paste)	None	138°F until hardened thence 180°F-16 hrs	¼ in sheets
MEK peroxide 1%	Cobalt naphth 1.5%	Room temperature 20 hours	Cement
MEK peroxide .5%	Accelerator"B" 1%	Room temp-16 hrs 180°F-16 hrs	5" OD x 1.5" thick cylinder
MEK peroxide .5%	Cobalt naphth 1%	Room temp-16 hrs 180°F-16 hrs	3" OD x 2" thick cylinder

Notes:

1. Cobalt naphthenate colors the resin a pink-blue color and cannot be used where a clear casting is required.

2. Percentages given for accelerators should be increased somewhat when new resin is used in which little of the inhibiter has been dissipated.

3. In general, when casting pieces larger than those mentioned, the catalyst concentrations should be reduced. It is best to err on the side of using too little catalyst.

After deciding on the catalysts to be used, the resin was carefully weighed and the catalysts added. It was found that this could best be accomplished in a one-pint sized paper cup. It is absolutely imperative that the catalyst be completely mixed with the resin. If not thoroughly mixed, the areas of high catalyst concentration will become hot spots during polymerization, causing cracking of the hardened plastic. The surfaces of the glass molds should be thoroughly clean and free from fingerprints. Silicone mold release, sprayed on by an aerosol spray, was used as the release agent. Best results were obtained using a minimal amount of lubricant. Any excess should be carefully wiped off, as it will lead to a foggy surface on the finished cast plates. The mold was assembled with the $\frac{1}{4}$ inch spacers separating the glass plates. The mold was then brought to a temperature of approximately 170°F for thirty minutes. The purpose of this was to soften the Plexiglass so as to obtain a better leakage seal for the mold. The catalyzed resin was then poured into the mold and the mold assembly placed in the oven. A Central Scientific Company De Khotinsky oven was used, but better results could probably be obtained in a

forced draft type drying oven. The principal difficulty experienced in this stage was the elimination of the numerous bubbles which form in the viscous resin mixture. After much experimentation, the following procedure gave excellent bubble free castings:

1. After mixing plastic resin and catalyst in paper cup, let stand for 30 minutes.

2. Pour into mold, attempting to have plastic run down side of mold, rather than drop through the air.

3. Let mold stand for 30 minutes.

4. Place filled mold in contact with a source of vibrations for from 3 to 4 minutes. The source of vibrations may be a jig saw, vibration fatigue machine, or similar tool. The vibrations settle the fluid in the mold and bring the bubbles to the surface.

After the filled mold has been in the oven for approximately 5 to 6 hours at the recommended temperature of 138°F polymerization will occur. The start of polymerization is indicated by gelling of the plastic. This process is accompanied by the evolution of a considerable amount of heat, and the mold was removed from the oven in order to allow the heat to be dissipated as rapidly as possible. When the resin mixture had solidified, the Plexiglass spacers were removed. This was done to avoid the marring of the surface which would occur if the plastic were allowed to shrink away from the glass plates. The mold was then returned to the oven and the temperature brought to 180°F. After curing for 16 hours the oven was slowly brought to room temperature and the mold removed. The plastic sheets produced were clear, with highly polished surfaces, and did not require annealing to free them from residual stresses.

The procedure for casting the blanks from which the circular cylinder model was machined was similar to that for the sheets. Because of the thickness of the piece, extreme care had to be taken to avoid thermal stresses which would crack the plastic during polymerization. Precautions taken included reducing the catalyst concentration as low as possible and allowing the plastic to solidify at room temperature. A 5 inch diameter tobacco can was used as the mold. Silicone mold lubricant was applied and the filled mold freed of bubbles by the vibration technique described previously. Even with the precautions taken, some small surface cracks were evident on the surfaces of the casting. These were later removed during the machining process.

The procedures outlined are those which gave the best results. Many variables, such as thickness of casting, amount of inhibiter still present in the resin, mold material, and air circulation in the oven, tend to make it impossible to cast the resin on a cook-book basis. When preparing models from a castable resin the investigator should be prepared to devote a considerable amount of time in perfecting a successful technique.

B. Machining.

The models fabricated from the $\frac{1}{4}$ inch cast sheets (Figure 2) were rough cut utilizing a conventional jig saw. Surfaces of the model were covered with masking tape to avoid marring. The tensile specimens were machined on a DuMore high speed grinder utilizing a $\frac{1}{4}$ inch diameter 48 tooth tungsten carbide cutter, operating at 22,000 RPM. The model, fastened to a .1 inch aluminum template, was guided against the high speed cutter utilizing a guide spindle in the base of the tool. The guide spindle is removable and, by the use of a .005 inch oversize spindle, permitted making a rough cut prior to the final light cut. This method of machining permitted making models, free of machining stresses, in a minimum of time. The technique is easily mastered and the services of a machinist are not required, except in the manufacture of the original templates. This operation produces a large amount of fine plastic dust which may cause headaches. The use of a vacuum dust collecting system is recommended.

The machining of holes in Paraplex P-43 probably presents the greatest machining problems. Stress concentrations arising around a drilled hole may severly distort the isochromatic fringe pattern in the model under test. Stress free holes were drilled utilizing drill speeds of from 700-1000 RPM. Extremely slow feed was used and the drill was frequently withdrawn and accumulated chips removed. Kerosene was used as a lubricant. The drills used were not reground. Since fully cured P-43 is extremely brittle, extreme care must be exercised when the tip of the drill breaks through to avoid chipping.

The cylindrical models were machined on a conventional metal

lathe. In order to avoid excessive machining stresses light cuts should be made. A finish cut of not more than .004 inch, and preferably .001 inch, is recommended. By the use of light cuts and sharp cutting tools the faces of the 4"OD x 1"-thick circular cylinder model were machined so that no further polishing was required to give satisfactory results.

The only model which required annealing was the 4" x 1" cylinder. After considerable experimentation the following procedure was established:

1. Immerse model in mineral oil. Heat to 175°F and hold for 12 hours.

2. Cool as slowly as possible to room temperature.

3. Heat to 240°F and hold for 4 to 6 hours.

4. Cool slowly to room temperature. If cooling rate is too fast, utilize metal blocks or some other means of retaining heat.

5. Examine under polariscope for residual stresses. If still present repeat process. The time at temperature in Step 3 varies with the thickness of the model. For models thicker than 1 inch the times should be increased over those recommended.

The mineral oil serves to give more uniform heating and cooling and also helps prevent the formation of edge effect stresses (21).

C. Installation of Thermocouples.

In order to determine temperatures within the models it was necessary to cement thermocouples directly into the model. Copper-constantan thermocouples of No. 30 wire (0.01") were used. Because of the low thermal conductivity of the model material, the smallest

practicable size thermocouple wire was selected in order to minimize heat transfer through the wire itself. Two types of thermocouple junctions were constructed. The first type, shown in Figure 21, was utilized in the 4" x 1" cylinder for temperature measurements at a preselected point. The head was formed by electrical arc welding in one arm of a mercury-filled tube. In order to get best results,it was necessary to remove the oxide film from the wire ends with a suitable abrasive. The wires were twisted together and welded. The surface of the mercury was covered with machine oil in order to quench the arc. The leads were then untwisted so that they were in contact only at the bead. The butt type junction (Figure 21) was used where it was desired to obtain an average temperature over the thermocouple length. The terms butt and parallel refer to the appearance of the wire before twisting. The wires were twisted as illustrated and soldered (22). The length of the junction should equal the thickness of the model in which it is to be imbedded.

The two principal requirements of the thermocouples embedded in the model are: that they provide an accurate indication of the temperature at the location where they are inserted; and that they have a minimum effect on the isochromatic fringe pattern. These requirements were fairly well satisfied by drilling a small hole in the model and cementing the thermocouple in place with Paraplex P-43 as the cementing agent. The thermocouple holes were drilled with a standard #53 high speed twist drill. The drill tip was not reground. A drill speed of approximately 700 RPM was used. Kerosene was employed as a coolant and lubricant. The drill feed was slow with the drill being removed from the work frequently to remove chips and to apply lubricant. Great care was taken to prevent overheating. The thermocouple leads were coated with the cementing medium and, after

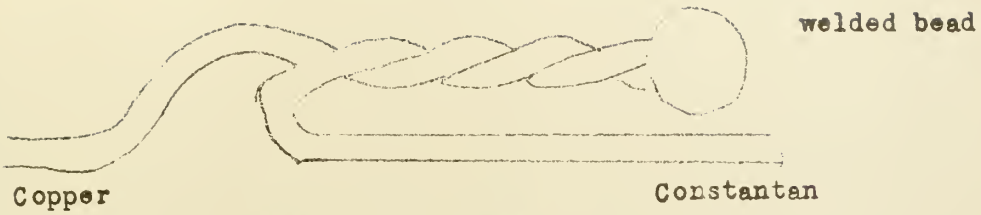

Parallel Type Thermocouple

Butt Type Junction

Figure 21 Thermocouple Junctions

curing, the coated lead was cemented into the hole. Best results were achieved using Paraplex P-43 with the room temperature cure catalyst combination; 1% MEK Peroxide, 1.5% cobalt naphthenate. The cement was allowed to cure overnight at room temperature.

D. Cementing of P-43 Models.

One of the reasons advanced for selecting Paraplex P-43 as a model material was the relative ease with which it can be cemented to form complex models. A preliminary investigation was made into the cementing of models using cements consisting of P-43 alone and a mixture of P-43 and P-13. Rohm and Haas Company also suggested the use of epoxy resins as a cementing medium (23).

Both P-43 alone and the mixture of P-43 and P-13 gave good bonds. Only a very small amount of cement is required. Best results were obtained with a catalyst which permitted room temperature cure. No pressure was required other than that necessary to hold the pieces together during the initial part of the cure. Average time for room temperature cure was 24 hours.

The composition for the(P-43)-(P-13) cement, as recommended by Rohm and Haas (24) is;

Parts by Weight	
75	Paraplex P-43
25	Paraplex P-13
1.0	MEK Peroxide
1.6	Cobalt naphthenate

The MEK peroxide and the cobalt naphthenate must be added separately, as they react violently when mixed together directly. The pink color of the cement is not noticeable when spread thin.

With care, joints were produced which introduced no distortion into the observed fringe patterns.